EV5V-CT94-0461

EARTHQUAKES PREDICTION IN TECTONIC ACTIVE AREAS USING SPACE TECHNIQUES

G. Luongo	Dip. di Geofisica e Vulcanologia, Facoltà di Scienze - Università Federico II di Napoli, Napoli, Italy
D. Ereditato	Dip. di Geofisica e Vulcanologia, Facoltà di Scienze - Università Federico II di Napoli, Napoli, Italy
G. Mucciacciaro	Dip. di Geofisica e Vulcanologia, Facoltà di Scienze - Università Federico II di Napoli, Napoli, Italy
F. Obrizzo	Osservatorio Vesuviano, Napoli, Italy
E. Cubellis	Osservatorio Vesuviano, Napoli, Italy
P. Hartl	Institut für Navigation - Universität Stuttgart, Stuttgart, Germany
K.-H. Thiel	Institut für Navigation - Universität Stuttgart, Stuttgart, Germany
D. Becker	Institut für Navigation - Universität Stuttgart, Stuttgart, Germany
M. Reich	Institut für Navigation - Universität Stuttgart, Stuttgart, Germany
J. L. Bles	Département Géophysique et Imagerie géologique, BRGM, Marseille, France
B. Sauret	Département Géophysique et Imagerie géologique, BRGM, Marseille, France
P. Murino	Dip. di Scienza e Ingegneria dello Spazio "L. G. Napolitano" - Università Federico II di Napoli, Napoli, Italy
M. Ferri	Dip. di Scienza e Ingegneria dello Spazio "L. G. Napolitano" - Università Federico II di Napoli, Napoli, Italy
L. Russo	Dip. di Scienza e Ingegneria dello Spazio "L. G. Napolitano" - Università Federico II di Napoli, Napoli, Italy
A. Fanelli	Dip. di Scienza e Ingegneria dello Spazio "L. G. Napolitano" - Università Federico II di Napoli, Napoli, Italy
L. Castellano	Dip. di Scienza e Ingegneria dello Spazio "L. G. Napolitano" - Università Federico II di Napoli, Napoli, Italy
R. Parente	Dip. Di Ingegneria dei Trasporti - Università Federico II di Napoli, Napoli, Italy
G. Alberti	Consorzio per la ricerca su sistemi di telesensori avanzati, CO.RI.S.T.A., Napoli, Italy
S. Mattei	Consorzio per la ricerca su sistemi di telesensori avanzati, CO.RI.S.T.A., Napoli, Italy
G. Rufino	Consorzio per la ricerca su sistemi di telesensori avanzati, CO.RI.S.T.A., Napoli, Italy
S. Esposito	Consorzio per la ricerca su sistemi di telesensori avanzati, CO.RI.S.T.A., Napoli, Italy

Abstract

This paper presents the results achieved in the framework of the European project "Earthquake prediction in tectonic active areas using space techniques" for forecasting earthquakes in the area of the Matese Mountains (Campano-Molisano Apennines).

The geodynamic processes which have produced the existent structural pattern of the Matese are analyzed in order to define the stress field acting in the area and derive a reliable model for the precesses of seismic energy release. The analysis is done on long term, by means of the study of the geodynamics processes which have affected the chain of Matese, and on medium-short term through the study of the historical and actual seimicity and of ground deformations which precede and accompany earthquakes. Thus, seismic and ground deformations monitoring systems have been carried out by the use of digital seismic stations, which integrate the existing seismic network, and of leveling route and tiltmeters for acquiring the slow ground motions. In addition, several GPS benchmarks and corner reflectors (CRs), triangular trihedron of alluminium, were deployed on the test-site to evaluate the capability of new space techniques such as GPS measurements and SAR Interferometry to measure terrain movements.

In our opinion the integration between data from monitoring, historical seismicity, geology and seismotectonic modelling of the area might realize the medium and short-term physical forecasting of earthquakes in the area of the Matese.

Keywords
Earthquake, prediction, SAR interferometry, GPS measurements

1. Introduction

The Matese complex, which extends from Isernia to Benevento is one of the most seismically active segments of the Apennine chain ((8); (29); (38); (39); (40); (55)). Within the geodynamical evolution of the Italian peninsula, and in particular of the Southern Apennine, the Matese complex is defined a transitional area since it is neither part of the Calabro Arch structure, nor part of the Umbro-Marchigiano-Toscano Arch. In fact, the significant variability of the deformations field shows not only the action of a complex regional stress field, but also a differentiation of the same one with respect to stress fields acting in the southern part and in the middle-northern part of the Apennines ((10); (13); (16); (21); (18); (28); (30); (32); (34); (37); (46); (47)). Consequently, in order to define the seismogenetic zones of the investigated area, it is necessary to analyse the local structures in a wider geodynamical contest, to better define both the limits of the different areas subject to stress fields and the interactions among them. This analysis is needed since the local data do not seem to be self-sufficient to define the seismically active areas and the ways of energy release. In fact the sources of major energy earthquakes seem to go through more surface tectonic structures and there is not a perfect correspondence between surface deformations and deep deformations. In addition, since energy accumulation and release occur on long time intervals, for those events that cross more tectonic structures, the processes that are behind the observed events are necessarily linked to large chain segments and, therefore, affected by stress fields on a regional rather than local scale.
In general, medium and short term earthquakes prediction is to be built on the interpretation of the processes that prepare the seismic event through the study of the so called precursors. Due to the complexity of the processes under way, this way will be efficient only if it is possible to get a reliable description of the stress field acting in the area of interest.
Our objective of earthquakes prediction on the Matese follows two directions: the first by monitoring of the ground defomations and seismicity; the second by the seismotectonic modelling of the area using historical seismicity, tectonics and geodynamical modelling of the area.
The integration between local data and regional modelling, has enabled us to formulate a preliminary seismotectonic model of the investigated area and to show the main relations between seismicity and tectonic structures, which is the first element to realize seismogenetics maps.

Historical and current seismicity

The Apennine seismicity clearly shows that the tectonic processes that have determined the current chain configuration are still under way. Yet, the distribution of earthquake foci and their dynamics cannot always be related to the surface geological structures. This item shows the complexity in reconstructing the stress field that has caused the present chain arrangement.
The focal mechanisms are mainly of dip slip kind for earthquakes of major energy and strike slip for the others ((13); (26); (54); (58); (61)). The dip slip mechanisms show the tensile axis perpendicular to the chain due to the rifting process migrating from the Tyrrhenic coast to the chain, while strike slip mechanisms can be related to strike slip movements perpendicular to the chain axis.
Also the composite mechanisms analysis of the seismic sequences of low energy of January 1986 localized at NE of the town of Isernia and that one of April 1990 a little north of the town of Benevento show that the tensile axis is aligned along the direction NE-SW, orthogonal to the chain ((4); (7)).
The pattern of the stress field obtained by the analysis of the deformations of pleistocenic sediments is coherent with the stress field tension obtained by focal mechanisms (16). The review of earthquake mechanisms of August 21, 1962 in Irpinia and the recurrence of sesmic events beneath sedimentary

intrapennine basins have induced Westaway (61) to believe that these basins are characterized by a high seismic risk. Also Lavecchia (30) shows a good correlation between the distribution of the main graben of the Miocene Early-Pleistocene of the Apennines and the seismic events with M≥6.5 occurred between the year 1000 and 1980 (Fig. 1). Yet, the focal mechanisms do not often describe the deformation fields expected in consequence of the geodynamical processes under way. According to Suhadolc et al. (58) this result may come from the action of local stress fields rather than regional ones in the hypothesis of plate tectonics.

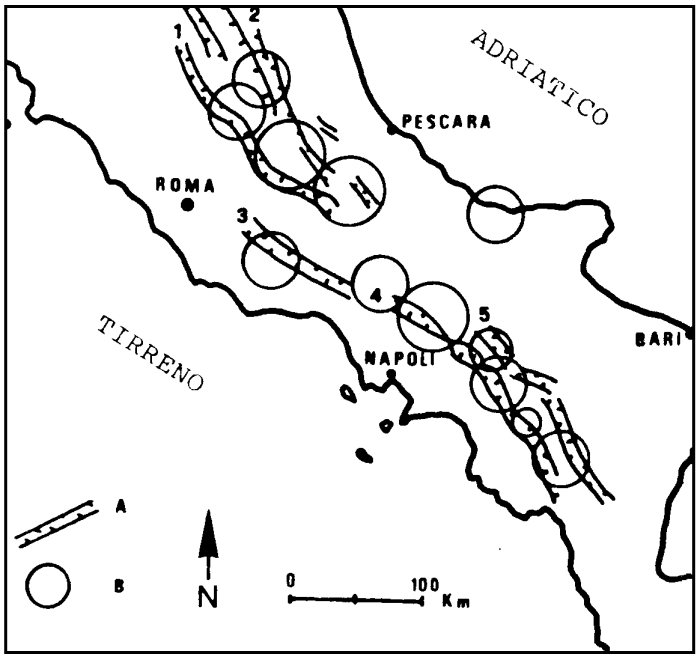

Fig. 1: Distribution of the main graben of the Miocene Early-Pleistocene of the Apennines and seismic events with M≥6.5 occurred among the year 1000 and 1980

The poor correlation between deformations observed in the chain and those resulted fom the analysis of the focal mechanisms can find a resonable explanation in the variations of the stress fields versus time. In fact, Hippolite et al. (28) by analysing the orientation of faults planes have shown that in the Early Pleistocene the maximum horizontal strain had the direction ENE-WSW and later the same changed in the direction NW-SE. In this more recent phase only deformations similar in extension to those observed by the focal mechanisms of the current seismicity can be found. The NE-SW extension invaded areas previously affected by compression.

The Campano Apennines is one among the areas in the Italian peninsula at highest seismicity ((11); (14); (48); (49)) (Fig. 2). Some earthquakes localized at the border between Campania and Molise and between Campania and Basilicata have caused damages on areas extended for thousands of square kilometers. The distribution of isoseismals above the VIII grade of the strongest earthquakes occurred in the Campano Apennines between 1456 and 1980 reveals that the seismogenetic areas are Matese, Sannio ed Irpinia.

This is one of the most active areas in Italy characterized by destructive earthquakes of magnitudo approximately 7. Most of these are localized on a narrow strip along the western summit of the Apennine chain with the alignment of the isoseismals of maximum intensity of historical earthquakes along the Apennine direction NW-SE, coherently with the distribution of the most significant tectonic features.

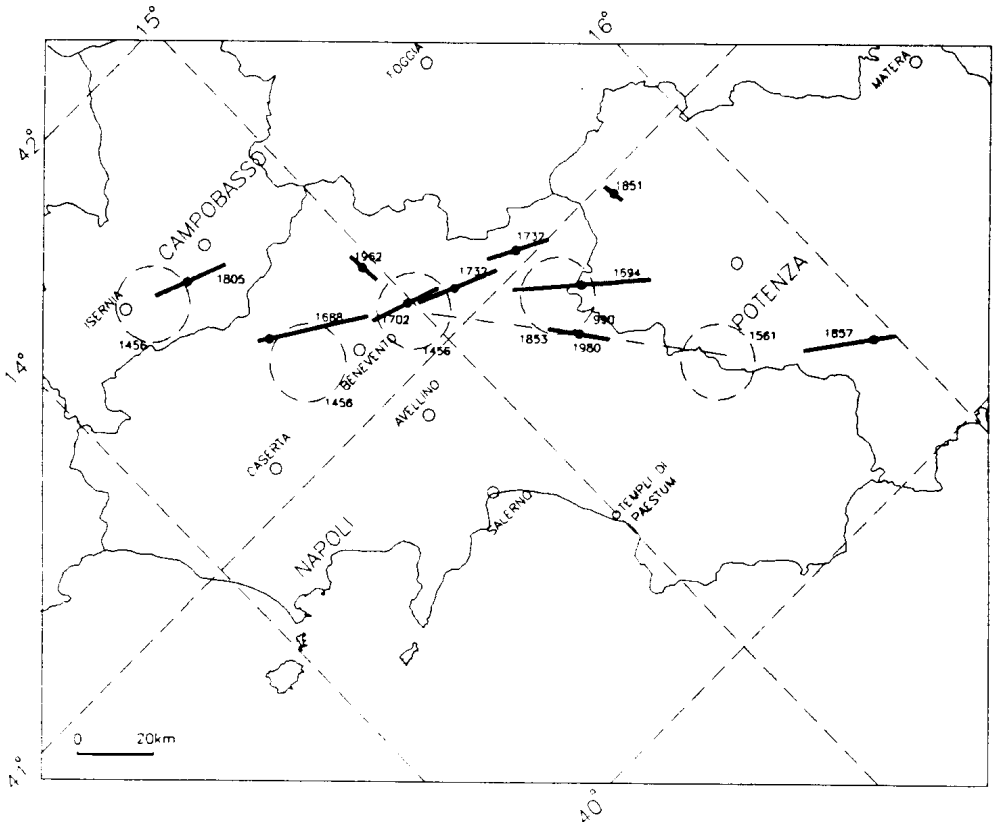

Fig. 2: The strongest earthquakes in the Campano Apennines starting from 1456 to 1980

It is therefore to believe that seismogenetic structures of the highest intensity earthquakes have a pattern along the longitudinal axis of the chain. The analysis of the historical seismicity in the area under investigation shows that:

- The isoseismals are clearly extended in the direction of the chain and follow the major tectonic features.
- The magnitude of hystorical events, assessed by comparing areas damaged by past and recent earthquakes, ranges from 6.2 and 7.5 (Table 1).
- The maximum length of seismogenetic faults reaches the value of 100 Km. (Table 1).
- Periods of seismic activity are separated by periods of inactivity sometimes very long.
- In major earthquakes complex rupture mechanisms are prevailing, as it can be inferred from the earthquake of 1456 (23). The many fractures in the medium accounts for the complexity of the rupture mechanism; the structures longitudinal to the chain can be significantly divided into fault segments that are generated by the rotation and migration of the peninsula towards Est.
- The structures transverse to the chain can be triggered by earthquakes along the axis of the chain itself, or they may have the function of channels of seismic energy. In this case the isoseismal would tend to rotate from the prevailing direction NW-SE to NS as observed relatively to the macroseismic field of the 26 July 1805 earthquake (20).
- The seismic activity is mostly found on the eastern side of Matese and the mechanisms are prevalently extensive with the main planes in the NW-SE direction.

The current seismicity in the Sannio Matese area presents frequent low energy earthquakes and its geographic distribution shows that the majority of earthquakes of moderate energy recorded in the period 1980-1991 is mostly found in a rather narrow strip of the peninsula, and have focal depths reaching up 20 Km (Fig. 3). As the analysis of the historical seismicity shows, the recent and present seismic activity is not related to a particular tectonic structure - the Apennine fault - on the contrary, the sources are various. A

confirmation of the complexity of the stress field acting and of the complexity of the seismogenetic structures generating seismic events of low or moderate energy is given by the analysis of the magnitudo-frequency distribution of earthquakes recorded in the period 1977-1987 which shows an high value of the "b" coefficient of the Gutemberg-Richter relationship. The most significant events were recorded in 1986 in the area of Isernia (Ml=4.0) and in the area of Benevento where the seismic crisis of April-May 1990 included events of low and moderate energy (maximum magnitudo 3.6) ((4); (5); (6); (7); (21)).

Year	*Day*	*Month*	*Magnitudo*	*L(Km.)*
1456	5	December	7.5	100
1688	5	June	6.8	45
1694	8	September	7.0	53
1732	29	November	6.8	45
1805	26	July	6.8	45
1857	16	December	7.0	53
1930	23	July	6.8	45
1980	23	November	6.8	45

Table 1: Earthquakes of major intensity recorded in historical times

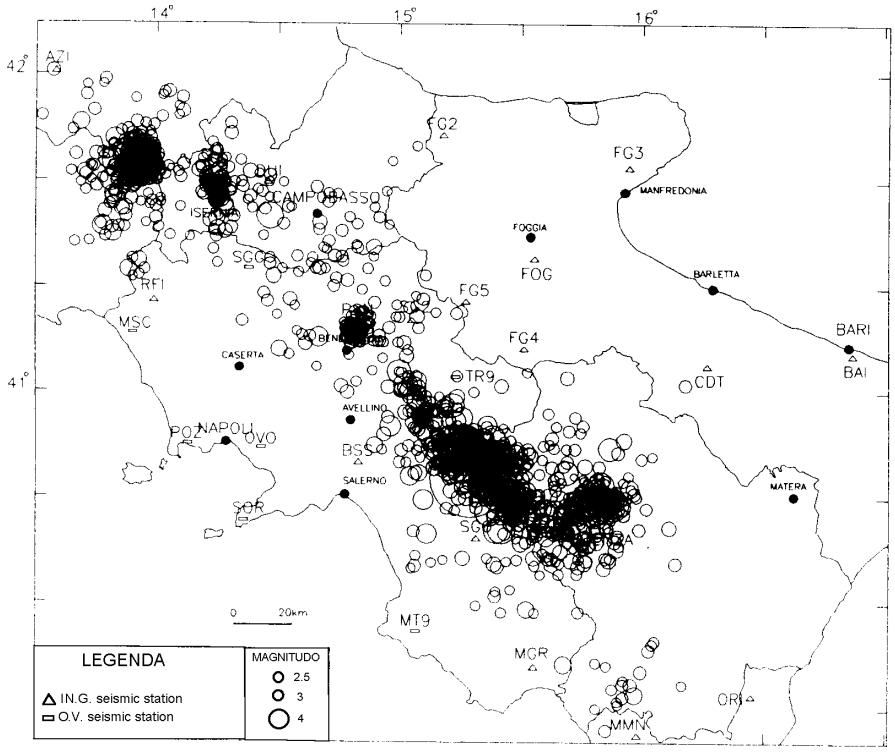

Fig. 3: The geographic distribution and the energy levels of the present seismic activity

In short, in this part of the Apennines which is defined transitional between the two arches, and which includes the Matese complex, it is possible to find four main seismogenetic areas with different seismic behaviour:

1) Southern Abruzzo, where seismic activity whether in historical times and in recent times shows mid-low level energy;
2) Molise, with historical earthquakes of high intensity (> X grade) and recent seismic activity with characteristics of low energy (Ml=4.0) in swarms;
3) Benevento, with historical earthquakes of high intensity (>X grade). It is to mention also the earthquake occurred in 1962 with intensity of IX grade (61), while the recent activity shows frequent and low energy events;

4) Campania-Basilicata with events of high level energy and intensity whether in historical and recent times. It is to mention in recent times the Irpinia earthquake occurred in 1980 (Ml=6.8).

Monitoring networks

The current deformations in the Matese area are measured through the study of seismicity and ground slow motions.

Seismicity is monitored through the stations of the national seismic network managed by ING (National Institute of Geophysics), the regional network of the OV (Vesuvian Observatory) and 4 temporary stations of DGV (Department of Geophysics and Volcanology) which were installed to reduce the gap of permament network stations (Fig. 4).

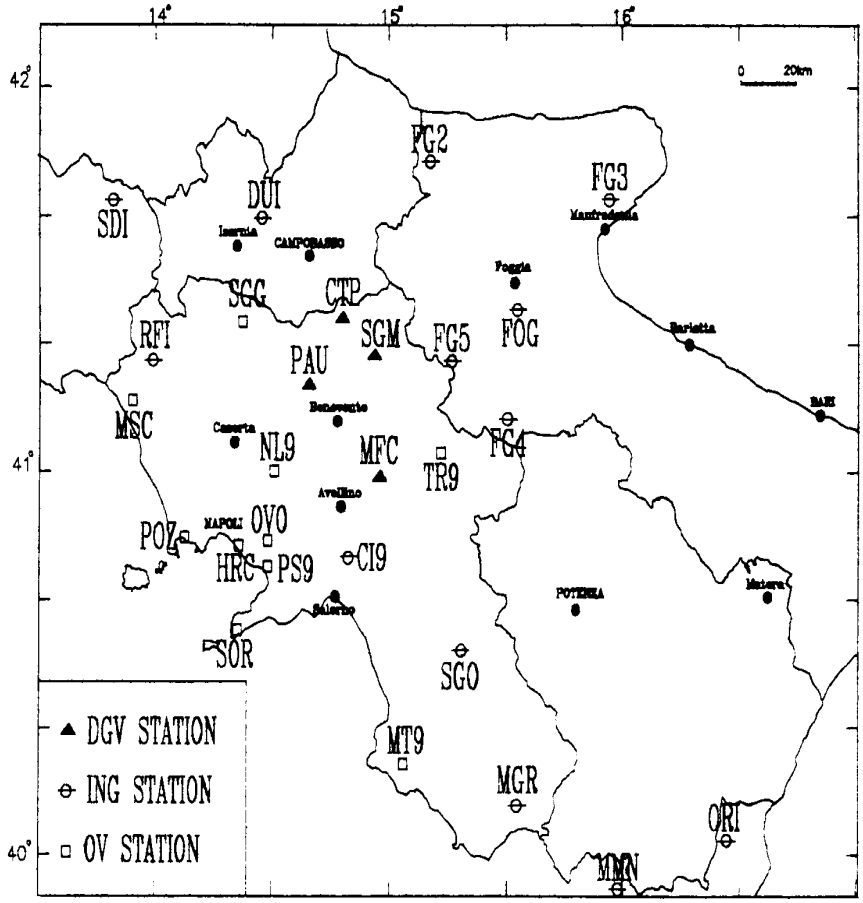

Fig. 4 - Seismic network

Slow ground motions are measured performing precision leveling and measures of ground inclination. A leveling route was carried out across the Matese Mountains and linked to the high precision leveling route of Italian Geographycal Military Institute (IGMI) in the Campania Plane ((15); (16)). To better define the frame of the slow ground motions, a tiltmeter station has been placed at Baia Latina (CE) on the Campano side of the Matese massif in proximity of the Dragoni GPS and of the leveling route.

In addition, the capabilty of Classical and Differential SAR Interferometry, and Global Positioning Systems(GPS) to measure ground motions has been evaluated by installing 20 CRs and 16 GPS benchmarks (Fig. 5).

The techniques that will be used have been selected with two objectives; from one side they are aimed to obtain results on the medium-long terms even without the occurrence of a significant seismic event, and from the other side on the short term in case of a seismic event.

Seismic and ground deformation monitoring

An analysis of the temporal series of the seismic events recorded by seismic network between 1985 and 1995 has showed that recent activity in the area is almost stationary. In fact, the energy released remains at constant values with events of magnitudo comprised mainly between 2.0 and 3.0 (Fig. 6). Also their spatial distribution does not show significant variations within the same time interval. The distribution of epicenters shows an alignment along the direction SE-NW, in agreement with the historical seismicity.

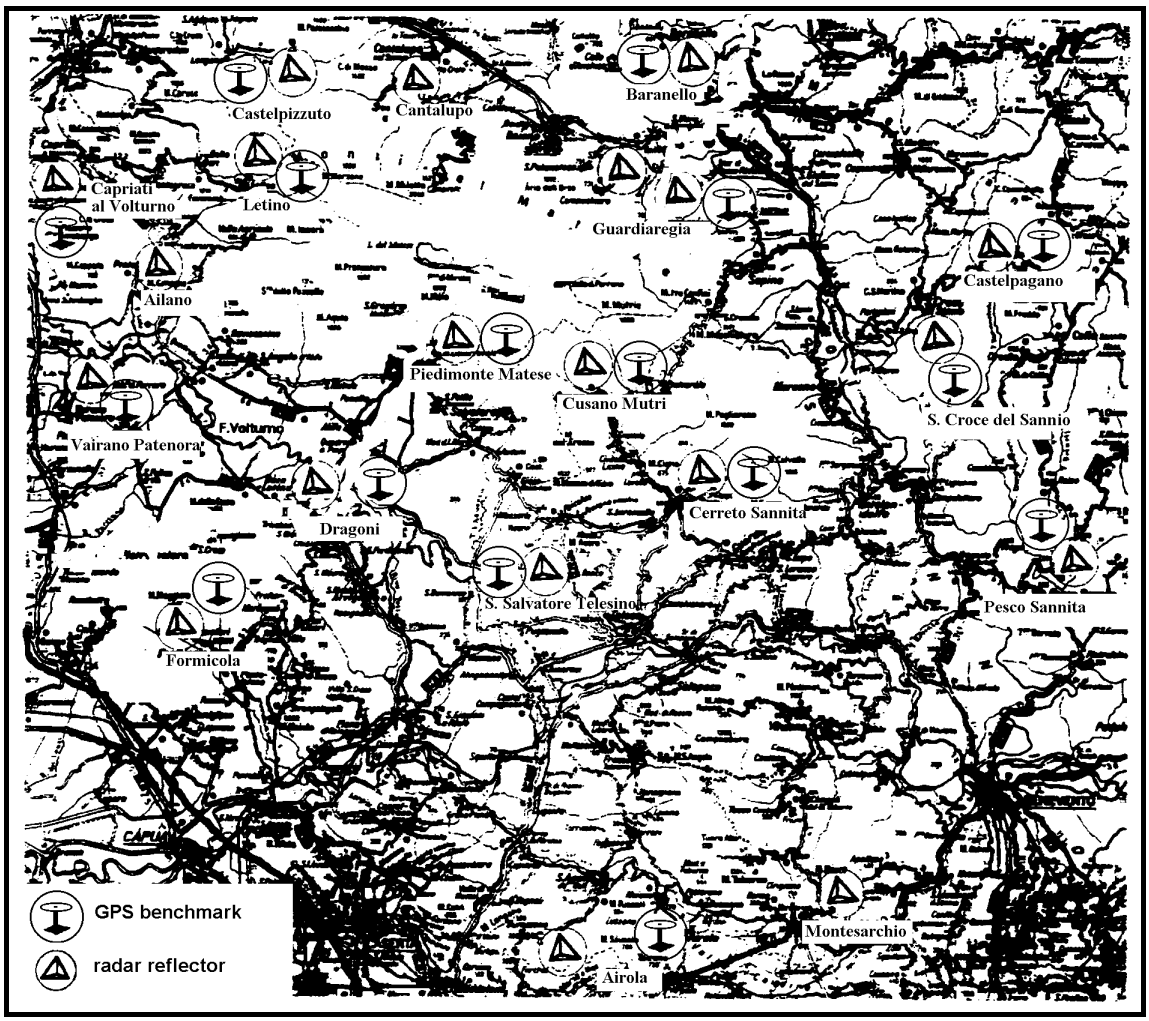

Fig. 5- CRs and GPS benchmarks installed on the test-site

At the same time, the ground deformation data recorded by a tiltmeter station installed at Baia Latina has confirmed that the area in exam was not subject to significative deformation during the period of observation.

As far as the leveling technique is concerned, a leveling route of km 125.300 was installed on area. Some deviations from the principal route was made to hook 5 GPS benchmarks (Dragoni, Piedimonte, Letino, Guardiaregia, Baranello). The total number of leveling benchmarks is 161 (106 vertical and 55 horizontal benchmarks) located on the basis of geological and structural knowledge of the area and so to be in contact

the main tectonic elements of Matese which could be involved in a dynamical process in concurrence with a seismic event.
This route starts from Taverna Spartimento (benchmark n. 47), crossing between the routes 22, 24 and 83 of the IGMI, follows the SS6 Casilina according to the path of the route 22 and then crosses the Piana Alifana and the Matese Mountains (Fig. 7).
A leveling campaign was carried out during this project using a electronic level "Leica Na3003" equipped with 2 Invar bar-code staffs.

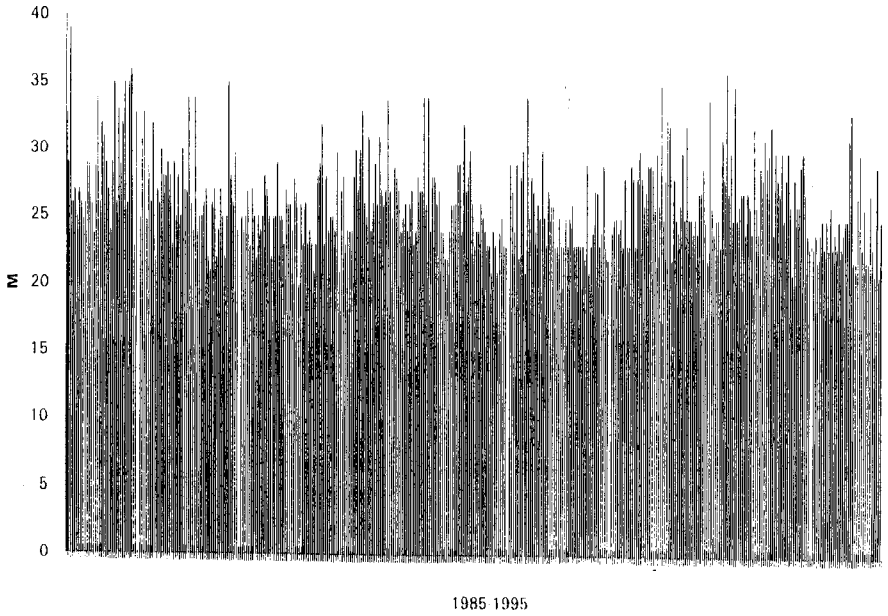

Fig. 6 - Magnitudo of the seismic events recorded from 1985 to 1995

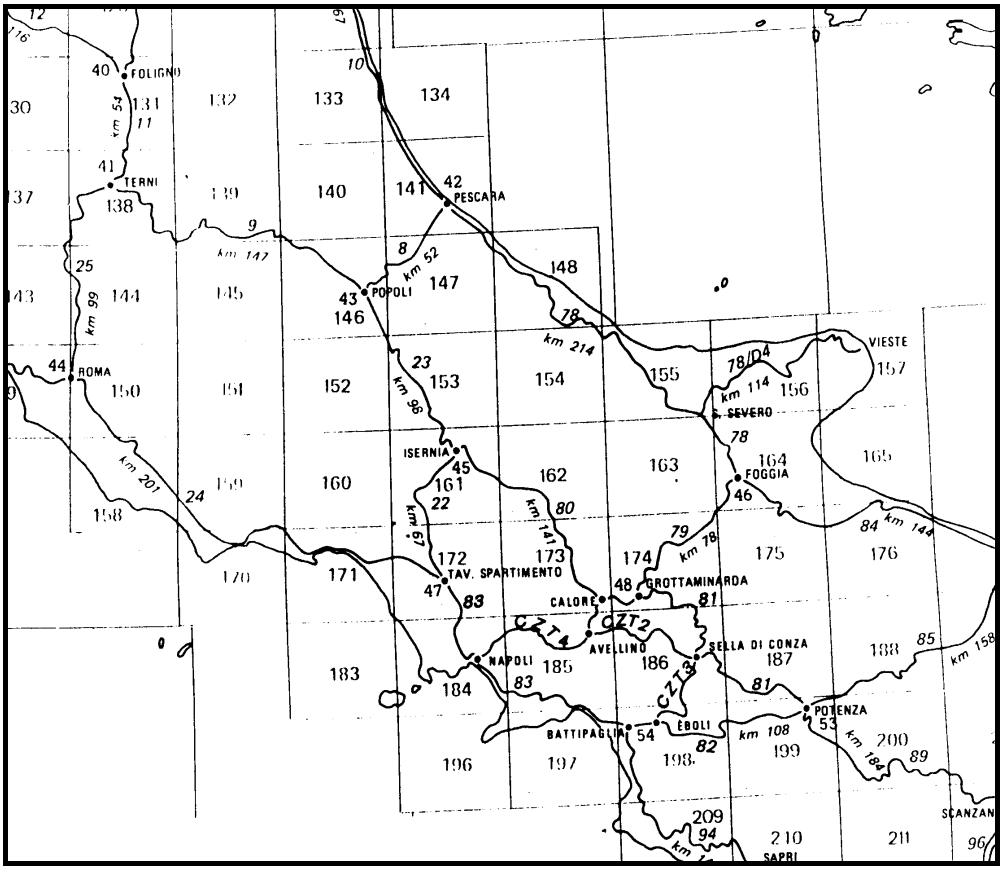

Fig. 7 - High precision leveling route of IGMI

GPS measurements

Measurements performed by GPS technique enables to determine with good precision the horizontal components of the displacements field.

The GPS network is formed by 16 3-D benchmarks (Fig. 5) more two additional fixed poles named A and B (Table 2), where the receiver could be operated automatically. Table 2 lists the names of the places where the benchmarks were installed and the relative labels. For obvious reasons, given the precision required by GPS control, these benchmarks were fixed to ground by excavation and use of concrete. In addition, in order to make GPS measurements more reliable and their repetition easier, forced centring poles of Gubellini type were used ((22); (59)).

BM no.	Name	BM no.	Name
1	Formicola	10	San Salvatore Telesino
2	Airola	11	Cerreto Sannita
3	Pesco Sannita	12	Santa Croce del Sannio
4	Castelpagno	13	Guardiaregia
5	Baranello	14	Letino
6	Castelpizzuto	15	Piedimonte Matese
7	Capriati a Volturno	16	Cusano Mutri
8	Vairano Paternora	A	Baia Latina
9	Dragoni	B	Pesco Sannita

Table 2 - Overview of the benchmarks in the Sannio-Matese area

In November 1994 a first GPS campaign was conducted on the area using 6 TRIMBLE 4000SSE receivers; two of them fixed and four mobile, for a continuous acquisition of about 6 hours each day.
The final coordinates of the two reference points A and B and of most part of benchmaks were computed. The geographic coordinates of the benchmarks number 1, 5 and 13 were not evaluated because the GPS-receiver got problems with respect to jamming signals. Therefore, these benchmarks had to be reinstalled for the second GPS campaign. The new monumentation was done at quasi interference-free' sites as close as possible to the old ones. In addition, the benchmark number 10 had to be changed because of stability problems. Accordingly to the old names, the new benchmarks were labeled with 1N, 5N, 13N and 10N.
The second GPS-campaign in the Sannio-Matese area took place in June/July 1995.
As in the first campaign, there were two additional fixed pole. Point A was the same pole at Baia Latina, whereas point B was shifted to the root of the town hall of Pesco Sannita about 30 m away from the old one. To distinguish between the different points A and B of the two campaigns, they were renamed A1 and B1 within the 2^{nd} campaign.
The second measurements were performed with some significant improvements in the measuring concepts and the network geometry. Thus, this second campaign has to be defined as new initialization data base with respect to the continuity of surveying in the future. Table 3 reports the final geographic coordinates of all benchmarks. The final adjustement (dn, de, dh) has been done with respect to the 'stable' benchmark 16.
The last GPS campaign was conducted in June 1996. During this experiment there was the chance to measure almost the same sub-networks as in the previous '95. As benchmark 4 was lost because of destruction, some small changes in the observation order were done in the northeastern part of network.
The two additional receivers were established at the same sites of the second GPS campaign and labeled A2 and B2 to separate the experiments because of the instable fixing of these points. As the monumentation of B has been improved meanwhile, here this convention is no longer necessary. With the other four receivers small sub-nets were measured.
As in the earlier campaigns the standard parameters for data acquisition were used. Daily sessions were performed during a period of 7 hours at a sampling of 30 seconds. The satellite tracking elevation cutoff angle during the registration was set to 15°.
As a result of the processing of the third campaign, Table 4 lists the three-dimensional geodetic coordinates of all measured benchmarks including their internal accuracy. The final adjustement has been done with respect to the 'stable' benchmark 2.

CAMPAIGN '95						
BM	Lat. [°]	Lon. [°]	Height [m]	dn [mm]	de [mm]	dh [mm]
00N1	41.16902696	14.36956187	109.376	3.8	3.1	8.6
0002	41.05581592	14.59302896	299.602	4.0	3.3	9.0
0003	41.25497555	14.83145322	468.210	3.9	3.1	8.5
0004	41.40134810	14.82439863	840.262	4.2	3.3	9.3
00N5	41.52731308	14.56257765	653.729	4.1	3.3	9.0
0006	41.52620703	14.29855770	1082.015	3.9	3.1	8.6
0007	41.48446191	14.11335312	228.214	4.7	3.8	9.9
0008	41.33468546	14.11578759	182.400	3.6	2.9	8.1
0009	41.28276603	14.29136231	148.657	3.2	2.6	7.4
0N10	41.22575212	14.48690642	133.207	3.9	3.1	8.6
0011	41.29148371	14.59117445	624.004	4.1	3.2	9.0
0012	41.39933951	14.74204189	825.935	4.0	3.2	8.8
0N13	41.44490284	14.56179748	738.239	3.8	3.1	8.4
0014	41.45387674	14.25267523	1095.451	3.7	3.0	8.3
0015	41.33995591	14.32973075	169.979	3.2	2.5	7.1
0016	41.34207163	14.50233925	550.693	0.0	0.0	0.0
A1	41.29008394	14.27328826	166.728			

B1	41.23439707	14.81093578	460.577

Table 3 - WGS-84 coordinates and their residuals of Campaign '95

CAMPAIGN '96						
BM	Lat. [°]	Lon. [°]	Height [m]	dn [mm]	de [mm]	dh [mm]
00N1	41.16892936	14.36948132	114.941	2.3	1.9	14.4
0002	41.05571839	14.59294862	305.197	0.	0.	0.
0003	41.25487847	14.83137250	473.195	2.4	2.0	14.9
00N5	41.52721586	14.56249672	659.251	2.9	2.3	17.5
0006	41.52610979	14.29847697	1087.590	2.6	2.1	15.9
0007	41.48436454	14.11327252	233.740	3.8	3.0	23.0
0008	41.33458789	14.11570691	187.940	2.6	2.1	16.1
0009	41.28266857	14.29128168	154.177	2.3	1.9	14.2
0N10	41.22565462	14.48682583	138.789	1.9	1.6	12.0
0011	41.29138645	14.59109367	629.569	2.2	1.8	13.5
0012	41.39924237	14.74196094	831.522	2.6	2.1	16.0
0N13	41.44480566	14.56171660	743.780	2.5	2.0	15.4
0014	41.45377935	14.25259451	1101.020	2.6	2.1	15.9
0015	41.33985846	14.32964996	175.520	2.3	1.9	14.5
0016	41.34197425	14.50225838	556.247	2.6	2.1	15.9
B2	41.23429981	14.81085488	466.153	2.0	1.6	12.2
A2	41.28998641	14.27320741	172.904			

Table 4 - WGS-84 coordinates and their residuals of Campaign '96

At this point, to compare the coordinates of this campaign with those of previous one, the latter coordinates were adjusted with respect to the benchmark 2. Table 5 shows the result of this adjustement.
In order to calculate the long-term variation of the benchmarks between the two surveys, the coordinate differences between epoch '95 and '96 were evaluated and listed in Table 6. The uncertainty of these variation is based on the a priori standard deviations of the single-campaigns, which appears very low.

CAMPAIGN '95						
BM	Lat. [°]	Lon. [°]	Height [m]	dn [mm]	de [mm]	dh [mm]
00N1	41.16892940	14.36948150	114.937	1.6	1.3	10.3
0002	41.05571839	14.59294862	305.197	0.	0.	0.
0003	41.25487836	14.83137252	473.195	1.5	1.2	9.5
00N5	41.52721601	14.56249671	659.281	1.7	1.4	10.8
0006	41.52610983	14.29847697	1087.530	1.7	1.4	11.2
0007	41.48436454	14.11327256	233.744	2.1	1.7	13.3
0008	41.33458793	14.11570718	187.931	1.6	1.3	10.5
0009	41.28266854	14.29128179	154.196	1.5	1.3	10.0
0N10	41.22565468	14.48682593	138.788	1.4	1.2	9.2
0011	41.29138639	14.59109382	629.578	1.4	1.1	9.2
0012	41.39924243	14.74196102	831.519	1.8	1.4	11.1
0N13	41.44480570	14.56171665	743.807	1.7	1.3	10.7
0014	41.45377942	14.25259459	1101.020	1.7	1.4	10.9
0015	41.33985850	14.32965017	175.510	1.5	1.2	9.8
0016	41.34197433	14.50225859	556.251	1.7	1.4	11.3
B2	41.23429986	14.81085509	466.148	1.3	1.0	8.2

A2	41.28998645	14.27320779	172.895

Table 5 - WGS-84 coordinates and their residuals of Campaign '95

BM	Δx (North) [m]	Δy (East) [m]	Δz (Up) [m]	sΔx [m]	sΔy [m]	sΔz [m]
00N1	-0.004	-0.015	0.004	0.003	0.002	0.017
0002	0.000	0.000	0.000	0.000	0.000	0.000
0003	0.012	-0.002	0.000	0.003	0.002	0.017
00N5	-0.017	0.001	-0.030	0.003	0.003	0.020
0006	-0.004	0.000	0.030	0.003	0.003	0.019
0007	0.000	-0.003	-0.004	0.004	0.003	0.026
0008	-0.004	-0.023	0.009	0.003	0.002	0.019
0009	0.003	-0.009	-0.019	0.003	0.002	0.017
0N10	-0.007	-0.008	0.001	0.002	0.002	0.015
0011	0.007	-0.013	-0.009	0.003	0.002	0.016
0012	-0.007	-0.007	0.003	0.003	0.003	0.019
0N13	-0.004	-0.004	-0.027	0.003	0.002	0.018
0014	-0.008	-0.007	0.000	0.003	0.003	0.019
0015	-0.004	-0.018	0.010	0.003	0.002	0.017
0016	-0.009	-0.018	-0.004	0.003	0.003	0.019
00B2	-0.006	-0.018	0.005	0.002	0.002	0.014

Table 6 - Variation of the benchmarks between Campaign '95 and '96

The values in Table 6 shows a relative horizontal displacements in the cm-level with small standard deviations in the range of same mm. Typical for GPS-results is the worse result in the height direction. The uncertainty of the detected height change is much higher than the detected variations. The standard deviation becomes greater due to the fact that both variation add up.
In conclusion, also the GPS measurements confirm the stability of the area in exam.

SAR interferometry

SAR data acquired by satellites have proved to be very useful in research fields related to geology. Techniques suitable to these ends are both classical and differential SAR interferometry. The former allows to obtain elevation, slope and discontinuity models of terrain ((3); (50); (60); (63)), which can be used to integrate the information extracted from geological maps. The latter is capable to detect small terrain height variations ((25); (51)) caused, for instance, by seimic activity.

To perform classical and differential SAR interferometry are necessary, respectively, two and three passes over the area of interest and no significant changes of scattering mechanism should occur in the viewed scene between the passes, thus mantaining high coherence. The availability of tandem acquisitions has increased the possibility to realise this condition, at least for classical interferometry, thanks to the short temporal separation (1 day is the present ground-site revisiting cycle) between two consecutive passes over the test area.

To assure a high coherence at least in punctual area also in case of long temporal interval between two SAR passes 20 CRs were installed on the test-site along ERS-1 and ERS-2 ascending orbits and, where it was possible, in proximity of the GPS benchmarks so as to have reference points of precisely known geographical localization (Fig. 5). They have been used: 1) as ground control points for geometric registration of radar image pairs; 2) as coherent targets with high Signal-to-Noise-Ratio for highly reliable radar measurements; 3) control points for the validation of the Digital Elevation Model (DEM) of terrain 4) reference points for the computation of the relative height variation.

Once CRs had been installed on the test area, the first step was to identify them in radar images, so that they could be exploited in further processing as reference points. Eleven of the installed CRs lay in the area selected for this activity of study. A preliminary localization of each CR in the radar image was done on the basis of a visual inspection that led to the identication of the area where the CR had been installed. Due to the presence of many bright points surrounding the approximate location, it was not possible to detect the CRs at this stage. Then, in an area of 2 x 2 km² centered on the approximate location, all pixel imaging point targets were selected applying the procedure suggested by Bruzzi et al. (12), and the radiometric characteristics (ISLR, PSLR, broadening both in range and azimuth) of all selected point targets were evaluated; finally in each area a point target could be identified as CR on the basis of the computed radiometric parameters, with the exception of one CR, which could not be identified in SLC images examined.

Table 7 reports the computed radiometric characteristics of the identified CRs and the results of the procedure of Bruzzi et al. (test 1 and test 2).

Corner Reflector	test 1	test 2	range			azimuth		
			broadening	ISLR (dB)	PSLR (dB)	broadening	ISLR (dB)	PSLR (dB)
Formicola	0.142	-0.809	-0.9 %	-11.85	-20.49	16.1 %	-7.94	-16.49
Baranello	0.105	-0.710	15.7 %	-7.44	-19.03	20.5 %	-8.79	-19.09
Castelpizzuto	0.157	-0.605	2.1 %	-8.05	-17.29	10.3 %	-8.81	-17.91
Capriati a V.	0.263	-0.658	4.6 %	-8.06	-14.13	11.8 %	-6.32	-13.67
Vairano P.	0.139	-0.792	11.4 %	-9.05	-19.34	9.6 %	-6.17	-13.64
Dragoni	0.130	-0.739	4.2 %	-9.31	-21.61	13.2 %	-10.58	-15.30
Cerreto S.	0.176	-0.735	-2.2 %	-4.95	-14.84	11.8 %	-5.44	-14.08
Guadiaregia 1	0.176	-0.735	5.8 %	-5.90	-13.92	6.7 %	-7.77	-14.37
Letino	0.166	-0.750	13.8 %	-6.26	-25.06	14.7 %	-7.27	-18.62
Cusano Mutri	0.157	-0.789	7.7 %	-6.75	-19.39	11.8 %	-8.65	-14.07
Guardiaregia 2	0.156	-0.807	0.9 %	-9.86	-19.57	13.2 %	-9.67	-36.68
Cantalupo	0.042	-0.750	10.7 %	-14.08	-24.67	12.5 %	-10.25	-22.37
Ailano	0.117	-0.779	5.2 %	-9.21	-17.38	10.3 %	-8.83	-20.02

Table 7 - Radiometric characteristics of identified CRs

Interferometric processing was performed using SAR SLC images produced by ESA/ESRIN, which several authors have proven to be adequate for interferometric applications ((51); (63)). The images relative to the tandem acquisition over the test-area in August, September, November 1995 and February and April 1996 were used (Table 8).

They were selected among all passes according to the criterion of finding sets of at least three passes, at shortest time interval, able to produce two interferograms with baselines suitable for interferometric applications. This introduces constraints on the component of the baseline B_{perp} perpendicular to the line of sight (50). In order to allow an efficient phase unwrapping, it is required that B_{perp} ranges from 50 m to 200 m in the case of ERS-1/ERS-2 radar systems and geometry of observation (height of flight and angle of incidence of line-of-sight). These bounds, in fact, assure that interferometric phase is correctly sampled and baseline decorrelation (31) is avoided (upper bound), while phase measurements are not destroyed by noise (lower bound). All tandem pairs selected by means of the baselines available at the ESA/ESRIN server met the baseline requirement while non-tandem pairs with adequate baseline were obtained by combining some images of the tandem pairs 2 and 3 and of the tandem pairs 1, 4 and 5.
The selected area for interferometric processing was a subset of a quadrant consisting of 9000 single-look azimuth pixels x 1900 single-look range pixels including 9 CRs (Formicola, Baranello, Castelpizzuto, Dragoni, Cerreto S., Guardiaregia 1, Letino, Guardiaregia 2, Cantalupo).

Tandem	ERS-1		ERS-2	
pair	orbit no.	date	orbit no.	date
1	21159	01 Ago 95	1486	02 Ago 95
2	21660	05 Sep 95	1987	06 Sep 95
3	22662	14 Nov 95	2989	15 Nov 95
4	24165	27 Feb 96	4492	28 Feb 96
5	24666	02 Apr 96	4993	03 Apr 96

Table 8 - Processed ERS tandem data: frame 819, track 129, quadrant 2.

The first step of interferogram formation is a preliminary course registration at pixel accuracy. Each interferometric pair was registered by means of a 2D rigid translation based on the previous localization of the 9 CRs. Our procedure for fine registration (42) is based on the automatic identification of a large number of Ground Control Points (GCPs) in addition to the already identified CRs. This task cannot be easily accomplished with SAR data covering large areas (19) and requires a careful strategy. To this end, each image was divided into 512 x 128 pixels subareas and for each subset the brightest point target was assumed as GCP. Subsequently, each subarea was 10 times oversampled by means of cubic B-splines and the subpixel shifts between homologous areas were computed using the cross-correlation of the GCP amplitudes. Finally, the geometric registration was performed by means of bicubic polynomials, whose coefficients were computed with least square approximation, using as input the subpixel shifts.
The range and azimuth shifts computed for the tandem pairs and non-tandem pairs are quite regular (translation and stretching) with the exception of the pairs that involve the ERS-1 pass of November; in this case the shifts are quite large and exibit a rotation between the images. This is due to an orbit misalignment which determines a not negligible baseline variation, as it will be demonstrated later.
A coherent multilook (5 looks in azimuth) was executed on the interferograms in order to give the maximum likelihood estimation of the phase (60); as a result, each pixel images an area approximately 20 x 20 m^2.
The interferograms presents large areas with high coherence in case of pairs corresponding to tandem acquisitions, but when non-tandem pairs were considered, most of the scene presented low coherence, due to relevant time separation between the two passes. Table 9 reports the baseline components, the temporal baseline and the correlation coefficien for each pair whose perpendicular baseline component, reported by the Interferometric Orbit Listings provided by ESA/ESRIN, mets the requirement.
To make possible differential interferometry it is necessary to identify a third coverage offering high correlation coefficients and satisfactory baseline with at least one of a tandem pair, provided that the tandem interferogram was satisfactory. Unfortunately we were not able to identify any satisfactory area, even considering relatively small subsets, in spite of the quite large data set. Consequently it was not possible to apply phase unwrapping and to produce differential interferograms, apart from very small and irregular areas, where neither GCPs nor geographic references were found. As a consequence, further processing was restricted to classical interferometry using tandem pairs and no activity of differential interferometry could be executed.

Interferometric pair				Baseline components (m)		Temporal baseline	Average correlation
sat.	date	sat.	date	$B_{//}$	$B_{\perp}$	(days)	coefficient
ERS-1	05 Sep 95	ERS-2	06 Sep 95	49	100	1	0.60
ERS-1	14 Nov 95	ERS-2	15 Nov 95	-7	91	1	0.54
ERS-1	05 Sep 95	ERS-1	14 Nov 95	-1	113	70	0.32
ERS-2	06 Sep 95	ERS-2	15 Nov 95	-58	105	70	0.40
ERS-1	01 Aug 95	ERS-2	02 Aug 95	20	56	1	0.50
ERS-1	27 Feb 96	ERS-2	28 Feb 96	114	190	1	0.61
ERS-1	02 Apr 96	ERS-2	03 Apr 96	52	120	1	0.46
ERS-1	01 Aug 95	ERS-1	27 Feb 96	-101	-52	210	0.39
ERS-1	01 Aug 95	ERS-2	28 Feb 96	13	138	211	0.38
ERS-1	01 Aug 95	ERS-1	02 Apr 96	-67	-83	245	0.24
ERS-2	02 Aug 95	ERS-1	27 Feb 96	-122	-109	209	0.24
ERS-2	02 Aug 95	ERS-2	28 Feb 96	-7	81	210	0.24
ERS-2	02 Aug 95	ERS-1	02 Apr 96	-89	-140	244	0.23
ERS-1	27 Feb 96	ERS-2	03 Apr 96	86	89	36	0.30
ERS-2	28 Feb 96	ERS-2	03 Apr 96	-28	-101	35	0.24

Table 9 - Selected interferometric pair and correlation coefficients

Our procedure of phase unwrapping consists of two steps. First, in order to avoid error propagation, it is necessary the identification of residuals, i.e. local errors in interferometric phase (27). Then we group them by enlarging a 2D window according to the residue spatial distribution. The adaptive research ends when a single area contains an equal number of positive and negative residuals and, consequently, it is cancelled (3).
The next step of the interferometric processing is the baseline estimation. This step is fundamental to derive height measurements and it needs the highest possible accuracy, since baseline uncertainties, together with phase noise, determine the major contribution to errors in computed heights ((42); (31)).
Our procedure for baseline estimation is based on ERS-1 and ERS-2 orbital data, in particular we used the Propagated State Vectors (PSVs), i.e. 5 satellite state vectors computed for each SLC image at approximately 2.5 second interval and listed in the CEOS formatted SLC header (leader file, platform position data record). The elements of the state vector are the components of the satellite position and velocity vectors with respect to a geocentric, Earth-fixed, right-handed reference frame. A fourth order polynomial is then computed for each component as a function of time. The interferometric baseline is given by the satellite separation when the antennas view the same target, that is when the target is in the range elevation planes of both antennas. We compute the corresponding orbital times at 1/PRF accuracy using the SLC images after coarse registration. The satellite state vectors are calculated using the polynomials and, then, the baseline components are computed. To this end, we adopt a right-handed reference frame, whose origin is coincident with one satellite position, vertical z-axis directed towards the Earth center and lateral y-axis perpendicular to the plane defined by spacecraft position and velocity vectors (Fig. 8). In addition, we compute also the baseline in-plane components, i.e. parallel and perpendicular to the line-of-sight (Table 10). The x, y, z components will be used as input of the procedure to compute terrain elevation, taking account of the baseline azimuth variation.
The baselines listed in Table 10 are almost constant along the azimuth direction with the exclusion of pair including ERS-1 14th November 1995 pass. In this case, by moving from the first azimuth line to the last one, a variation of about 7 m was computed in the baseline y-component (Table 11), which means that the considered passage was not perfectly parallel to the others.

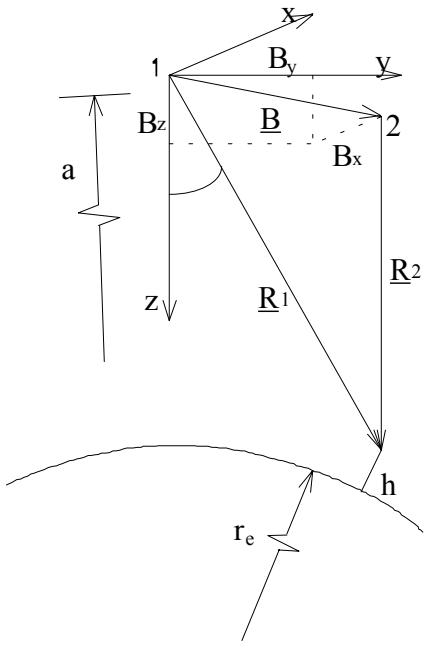

Fig. 8 - Geometry of observation

Tandem pair	Baseline components (m)				
	B_X	B_Y	B_Z	$B_{//}$	$B_\perp$
1	46.8	57.8	-1.6	16.3	55.4
2	888.5	117.0	15.3	58.0	109.0
3	74.0	-80.9	39.1	-12.2	89.0
4	-9.3	218.7	40.6	106.0	195.5
5	2.6	131.1	7.7	47.9	122.3

Table 10 - Baseline components computed at scene center

line no.	ERS-1 Nov. 95/ERS-2 Nov. 95		
	B_x (m)	B_y (m)	B_z (m)
1	77.888	-84.886	39.123
1001	77.565	-83.994	39.129
2001	77.222	-83.100	39.135
3001	76.862	-82.208	39.141
4001	76.489	-81.316	39.147
5001	76.106	-80.423	39.153
6001	75.719	-79.531	39.159
7001	75.330	-78.639	39.166
8001	74.945	-77.746	39.173
9000	74.569	-76.855	39.180

Table 11 - November 1995 tandem pair: computed baseline components as a function of azimuth position.

The analysis of the corresponding interferogram (Fig. 9) led a confirmation of these results. In fact, it showed interferometric fringes over flat areas (when detectable in spite of low coherence) not aligned along the azimuth (flight) direction, which can be interpreted as an effect of baseline variation as a fuction of azimuth position.To gain further insight a coarse analysis of baseline variation's effect on interferometric phase was performed: for a viewing geometry similar to the one over the area of interest, the difference of round-trip path satellite-target-satellite was evaluated in correspondence of baselines relative to first and last line of several interferograms; then the variation of path difference in terms of number of wavelenght, i.e. number of fringes along azimuth direction, per 100 lines of interferogram was computed and compared to the values deduced from the visual analysis of interferograms, finding that they are coincident.
To avoid decorrelation problems and speed up the processing, we decided to limit our activities to subsets where adequate correlation coefficients were available. A subset (about 10 x 10 km^2, corresponding to 512 x 512 pixels) centered on a flat area near Guardiaregia was selected and the interferometric data of the tandem pairs 1, 3, 4 and 5 were used.
With reference to Fig. 9 the height (h) of each pixel above a local spherical Earth (radius r_e) was computed as follows:

$$h = \left[a - R_1 \cos\theta \right)^2 + R_1 \sin\theta \right)^2 \right]^{1/2} - r_e$$

where a is the orbit semi-major axis and θ is the side looking angle related to the interferometric phase difference Φ by:

$$\Phi = \frac{2\pi}{\lambda} 2 R_1 - R_2 \right) \frac{4\pi}{\lambda} B_z \cos\theta - B_y \sin\theta \right) \frac{B^2}{2R_1}$$

where λ is the wavelength and the slant range difference was approximated by baseline second order Taylor series.
The area in exam comprises 3 CRs (Guardiaregia 1, Guardiaregia 2 and Baranello of known geographical localization provided by GPS) and 3 more GCPs. These reference points were exactly located also on topographic maps and were uniformly distributed across the scene. Although the CRs radiometric quality was limited and obviously the 3 additional GCPs were not exactly bright man-made point targets, the availability of reference points will be extremely useful to check the computed height quantitatively and to refine the baseline estimation, as it will be shown in the following. Finally, Fig. 9 depicts the interferograms obtained from the tandem pairs 3 and 4 and Table 12 reports the correlation coefficient of the selected subset.

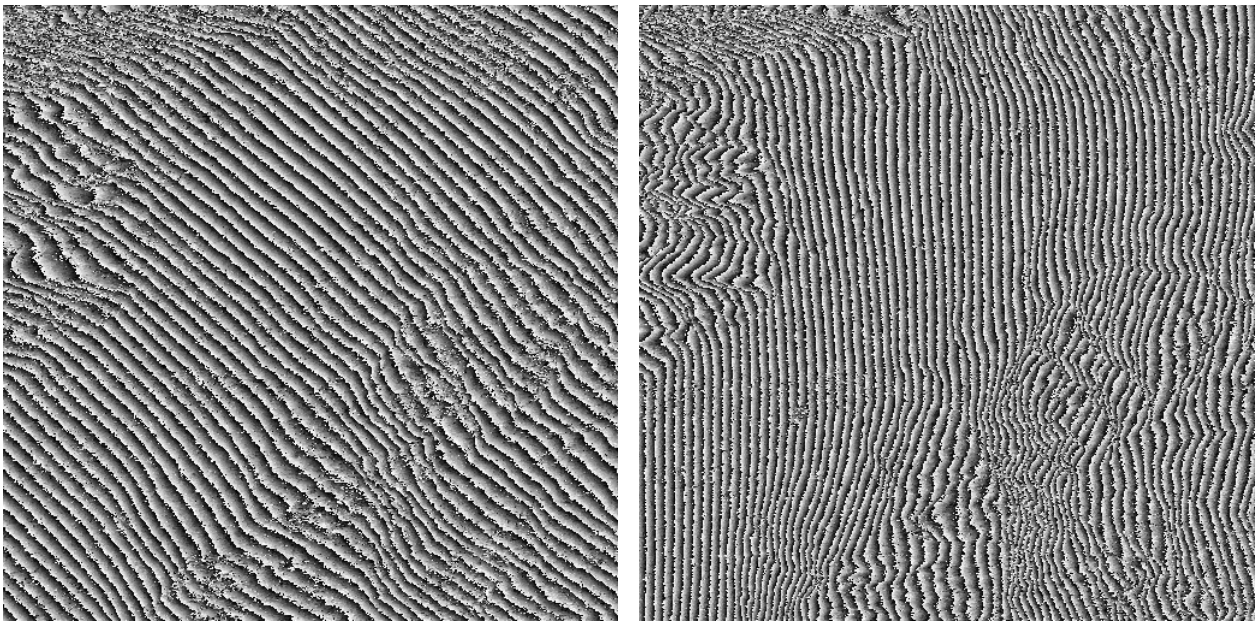

(a) (b)

Fig. 9 - (a) Interferogram of a subset extracted from tandem pair 3 with a flat areas in the middle; (b) interferogram of the same subset extracted from tandem pair 4.

At this point, the DEM was computed and the root mean square (rms) GCP heigth error is shown in Table 13. The rms error was evaluated using only the 4 GCPs not included in the regions cancelled out by the phase unwrapping procedure.
As shown by Moccia et al. (42), one of the most significant height error sources is the baseline uncertainty, which in our procedure is consequent to an inaccurate estimation of satellite positions. In particular, a constant error in baseline estimation causes an incorrect solution of the 2π ambiguity and, consequently, an error propagation in across-track direction, while an erroneous baseline time derivative introduces an inexistent slope in along-track direction. Several authors proposed original techniques to remove the above inaccuracies. As an example, Zebker et al. (63) modified the interferometric phase by means of a constant and a linear term computed using tie points. In 1993, Small et al. (56) introduced a method for computing a phase constant, an azimuth convergence factor and two constant baseline components for precise baseline estimation using tie points well-distributed across the scene. Our procedure is aimed at the improvement of the 2π ambiguity solution and at the refinement of the estimation of one baseline time-varying component using the GCP heights.

Tandem pair	Average correlation coefficient
1	0.57
3	0.62
4	0.68
5	0.56

Table 12 - Average correlation coefficients

Tandem pair	DEM rms GCP height error (m)
1	104.1
3	12.6
4	8.9
5	53.9

Table 13 - Rms height errors on the GCPs

As shown by equation of the interferometric phase difference, the most relevant contribution is given by the B_Z and B_Y inaccuracies, whereas the B_X component is less important. Furthermore, the computed B_Z variations are negligible with respect to the B_Y ones. Therefore our strategy was based on the minimization of the GCP height errors in a least square sense, by adding a linear term to B_Y in azimuth direction and a constant term to the 2π cycles. Table 14 shows the results obtained after the application of the procedure. In all the cases the procedure worked properly, requiring limited corrections. In particular, in tandem pairs 3 and 4 we obtained results comparable to the ones presented by Zebker et al. (63).

Tandem pair	By maximum correction (cm)	2π ambiguity correction (cycles)	Refined DEM rms GCP height error (m)
1	+3.0	+39	26.8
3	-1.8	-4	4.8
4	+4.4	-5	3.4
5	+8.0	+2	7.9

Table 14 - Height errors on the GCPs after the corrections.

Then we performed a comparison of the DEMs, obtaining a root mean square difference of 18.7 m in the best case (tandem 3 and 4). This less effective result is obviously due to temporal decorrelation of extended areas with respect to point targets, as pointed out also by Small et al. (57), who attained 2.7 m as rms height error on a comparably large area when correlation was instead greater than 0.8. For the sake of clarity, in Fig. 10 a, b 16 x 16 DEM pixels were averaged to plot a single height point. Fig. 10 shows also the areas cancelled by the unwrapping procedure.

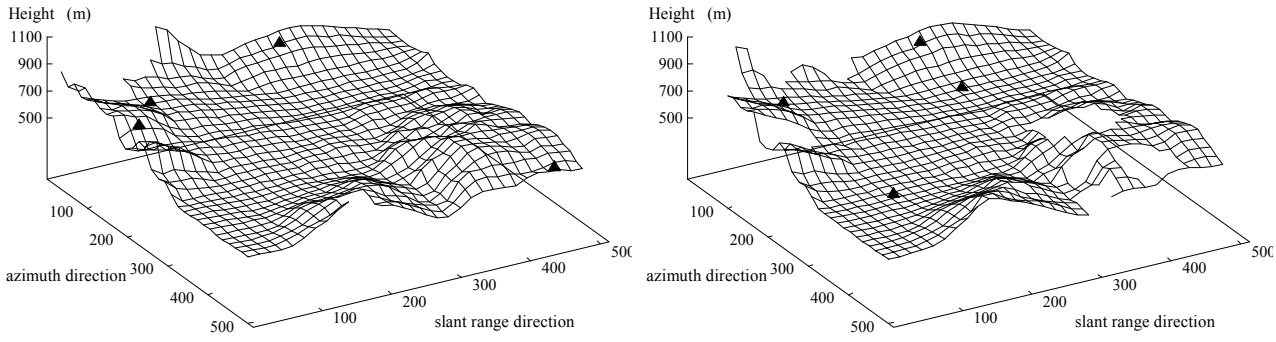

(a) (b)

Fig. 10 - DEMs of the interferometric pairs: 3 (a) and 4 (b). Triangles show the available GCPs.

The procedure for DEM production applied to the tandem pairs 1 and 5 required additional processing steps. Since the average correlation coefficients were 0.50 on the whole scene and only 0.57 on the selected subset in the best case, the phase unwrapping procedure identified a large number of residuals and cancelled large areas, making impossible an adequate DEM production. To avoid this problem an additional coherent multilook was applied (2 azimuth looks and 2 range looks). As a result, larger rms height errors on the GCPs were obtained (26.8 m and 7.9 m) with respect to the tandem pairs 3 and 4 (Table 14). With reference to the DEMs, Table 15 lists the rms height differences between all available DEM pairs. As expected, the tandem pairs with low correlation present large variances.

Tandem pairs		Rms height difference (m)	Time separation of tandem passes (days)
1	3	30.5	105

1	4	31.9	210
1	5	40.8	245
3	4	18.7	105
3	5	33.8	140
4	5	25.6	35

Table 15 - Comparison of the DEMs obtained from the available tandem pairs

In conclusion, the accuracy of the final product was satisfactory if tandem data were utilized. In fact, a rms errors of the order of 4 m were obtained in the best case (November 1995, February 1996), values comparable to the results presented by other authors in different condition.
As far as the Differential SAR Interforometry is concerned, the results show that the low coherence on large areas of interferogram when the repeat cycle was longer than 1 day did not allow to perform the tecnique. The coherence was so low that the unwrapping procedure could not even applied in corrispondence of the CRs only.
To overcome the problem of the low coherence, a further research on applications of differential interferometry could be performed focusing attention on a smaller test-area where a higher number of CRs should be installed, so that interferometric phase could be correctely sampled by means of measurements on CRs only, even if high coherence cannot be achieved. Anyway, it is important to stress that such a kind of experiment could not be performed aiming to collect information on phenomena which are precursory of seismic events, since, in that case, the test area must be large.
Notwithstanding the low coherency, the last chance to unwrapp the CRs interferometric phase could be offered by use of the digitalised scatterer elevation points of the test-area given by the Italian Istituto Geografico Militare (IGMI). The proposed approach is based on the use of a simulation program which has as input the digital terrain model of the area of interest and accounts for the satellite dynamic and the SAR pointing geometry.
The research activity of the next months will be focused on assessment of phase error introduced by this procedure.

Geological analysis of the Sannio-Matese area using SPOT and ERS-1/ERS-2 SAR images
The area under investigation has been interpreted from a geologic point of view by means of a SPOT image and ERS-1/ERS-2 SAR images.
The interpretation of the SPOT image has showed the following characteristics:

- Similarly to the Matese massif, the main faults of the calcareous massifs (Maggiore, Camposauro and Taburno), indicated on geologic maps, are easily found; they can be similarly detected, although less clearly, inside flysch units and inside Miocene formations.
- Inside the units of Sannio, the SPOT image allows to detect different lineaments and morfologic blowholes; those lineaments would seem to be the extension towards East of Matese faults.
- Est of Matese the N-S fault of Cerreto-Sannita visible on the image, seems to limit towards West the thrusting of the Sannio unit. It can be seen a scarp that could have acted during the Quaternary.
- On the edge of the Volturno-Calore depression seems that the fault of the Northern edge of Camposauro Massif would extend itself towards the massif of Mount Maggiore;
- West of the Taburno massif, a NW-SE fault near Melizzano is placed inside the extension of one fault on the Southern border of this massif. This fault near Melizzano interests calcareous tufa and would seem to interrupt a glacial torrent.
- On the Southern border of the Taburno massif, faults that interest quaternary glaciers show clearly on SPOT images.
- Faults that surround the Northern border of the Avella massif seem to continue towards N-W inside the Tairano massif, S-W of Airola.

The investigated area by means of ERS-1/ERS-2 SAR images covers about 2600km^2.The Matese massif is situated between the central and Southern part of the Apennines orogenic segments. This area is characterized by outcropping of quaternary deposits, neritic facies of the "Abruzzese-Campana" shelf, pelagic terrains of the "Molisano basin", flysch facies of the "Samnitic domain" and basin facies of "Sicilidi

unit". All these units belong to the succession of thrust nappes with Adriatic vergence of the sud-apennine chain.
The present set up of Matese massif is the result of the interaction between the Miocenic tectogenesis and extensional Plio-Quaternary tectonics.
The ERS-1 SAR ascending power image of January 31, 1995 and the ERS-2 SAR descending power image of February 22, 1996 acquired on the Matese area have been analyzed by computer assisted photointerpretation techniques.
Brightness, texture and shading have been considered to identify several features and lithologies, as well as the principal structural lineaments of the area. The geological map of the area has been used to compare and integrate the results of the analyses.
ERS-1 ascending pass image is the most suitable for the geological analysis of the Matese area since the radar illumination is quasi orthogonal to the main morphostructures of the massif. It is noteworthy to mention the correspondence between the geological formations and structures seen in the image and the geological map.
The analysis has allowed the identification of the limestones of Matese, Taburno, Camposauro and Maggiore Mounts. At the same time the basin and terrigenous facies of the molise-samnite units have been recognized as well as recent alluvial deposits (Fig. 11).
The Matese massif is affected by fragile deformations. The main structural lineaments inferred from the analysis of the images are drew in a skecht map (Fig. 12).
Foreshortening and layover can assist the interpreter in identifying neotectonic discontinuities, characterized by great throw and quasi-vertical slopes. These side faults, although eroded, retain a high slope and then they can be visualized in SAR images.
The geological map shows that a network of apenninic and anti-apenninic faults cross the Matese mountains. The most evident structures (in addition to the bordering ones) in the SAR images are those which cut the Matese Mountains in NW-SE direction.
In particular the Matese-Lake-Letino (F2) and Cusano Mutri-Capriati al Volturno (F1) structures are well visible: they divide the massif into three big blocks, northern, central and southern (Fig. 12).
SAR images seem to show that the three blocks of the massif are displaced one with respect to the others. It is reasonable to suppose a left strike component of the high angle faults which cut the massif. An example of this left transtensions can be the depressions of Letino and Matese lake.
Northwards, the Sepino-Cantalupo (F3) structure displaces the Samnitic thrust nappes by raising the SW block with respect to the NE one. Moreover, the N-S Cerreto Sannita-Guardiaregia vertical fault (F4) seems to highlight the superimposition of the "Samnite" and "Sicilidi" units on the rocks of the Eastern Matese.
The analysis of the seismicity suggests that the active structures are prevalently concentrated along the apenninic direction bordering the north-east side Matese and along the transversal structure Sepino-Cerreto Sannita.
A different mechanical behaviour of the crust can explain the seismic "silence" of the campanian side of the Matese massif. Some authors, interpret the Eastern and Western portion of the Matese massif as two superimposed platform dominions; the basin interposed between these dominions should be obliterated.
If this is the case, the ductile terrains of the basin should be located deeply to the south of Matese massif. If the strain velocity is very low, these terrains does not allow a strong accumulation of stress, and the seismic energy can be dissipated by creep phenomena. In this way, the absence of superficial earthquakes could be explained, but nothing can be deduced about deep ones.

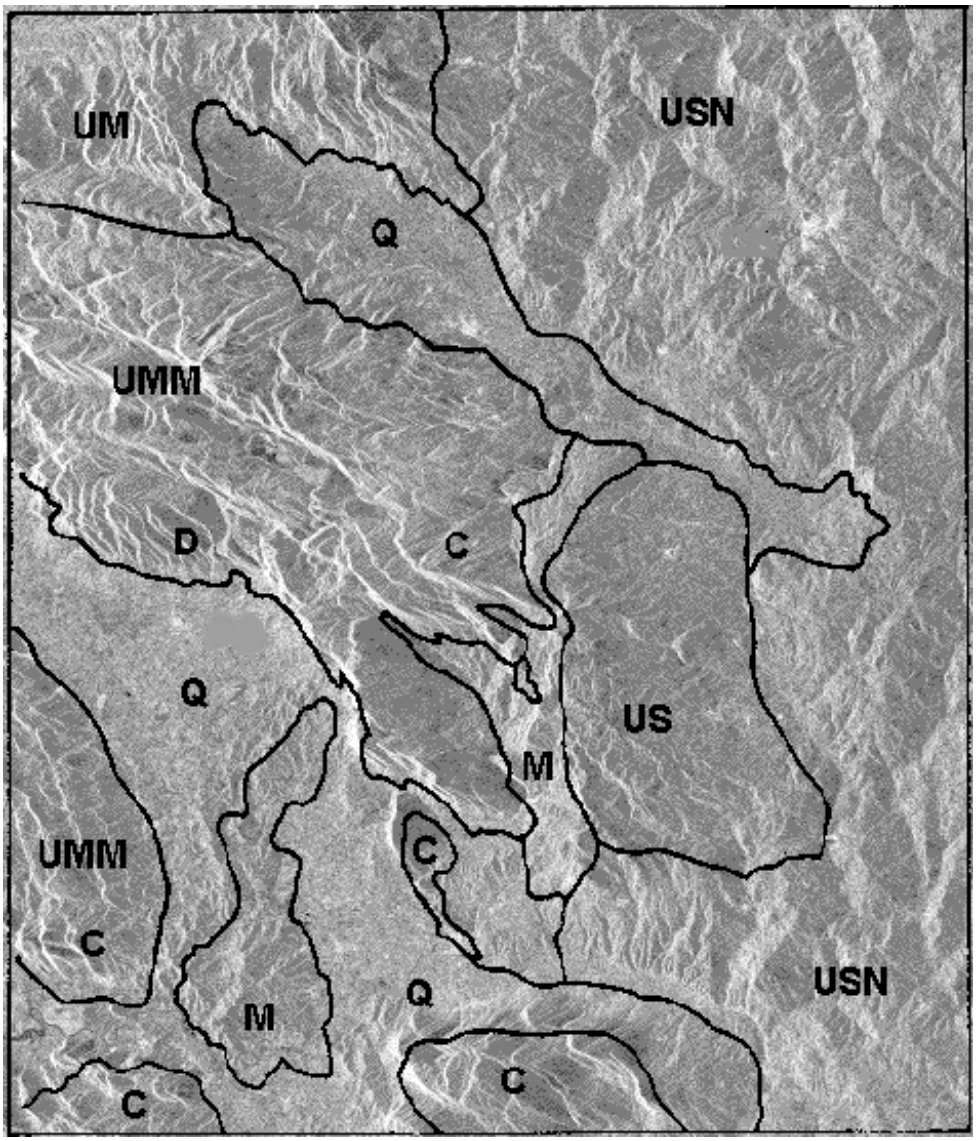

Q Quaternary deposit	US Sicilidi Unit
D Dolomite	UM Molisane Unit
USN Samnitic Unit	M Miocenic facies
UMM Matese Mount Maggiore Unit	C Limestones

Fig. 11 - Limits of the stratigraphic-structural units from the ERS-1 image

The "sicilidi" unit is formed by limestones, clays and marl and it is affected by numerous faults. SAR images show only a few linear features, probably due to a low inclination, in the average, of the fault side that is a consequence of the lithology type (clay and marl are eroded easily).
The descending image can complete the description carried out using the ascending image: in fact, it allows to analyze other slopes and identify features not visible in the ascending image because of the viewing geometry.
The simoultaneous ascending and descending orbits imagery allow to evaluate the asymmetry of the sides.
Considering that the Apennine is a recent orogene, the side having direction of dip of layers opposite to the slope of the same sides (planned on faults and modified by erosional processes) are usually steeper than the stratum side. Consequently the attitude of the layers can be inferred from the asymmetry of the slopes. The attitude of layers of the massif and of "Sicilidi" block is eastward.
Vertical faults that affected the molise basin are more evident on the ascending image because the western slopes are more inclined with respect to the eastern slopes.

The variations of texture among terrains having a different mechanical behavior are not well visible on the side along the incidence beam.

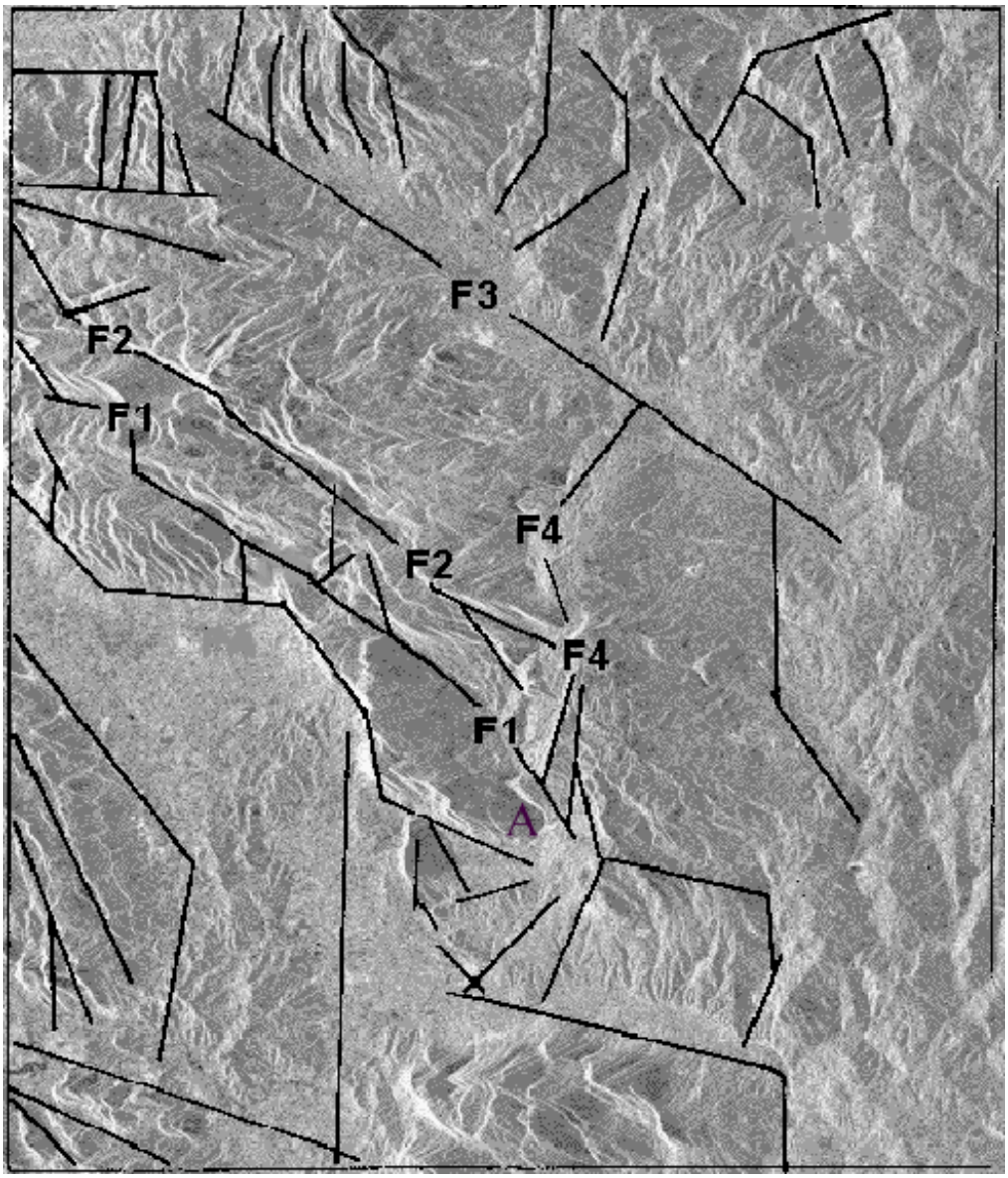

/= Principal structural lineament
F1 Cusano Mutri - Capriati al Volturno structure
F2 Matese Lake - Letino structure
F3 Cantalupo del Sannio - Sepino structure
F4 Cerreto Sannita - Guardiaregia structure

Fig. 12 - Principal structural lineaments.

Only to a great scale there is correspondence between texture, morphology and lithology on radar images. The point A on the image of Fig. 12 seems to belong to the flysch facies but actually this small block belongs to the Cretaceous limestones. The white lineament which marks the boundary is due to a strong backscatter caused by a reversal slope.

Analysis of the deformation of the Apennine-Tyrrhenian System and geodynamical model

The Apennine chain is formed by a thick pile of mantles of age comprised between the Trias and the Pliocene which after or during their formation have undergone important horizontal traslations and/or rotations characterized by repeated overlapping towards Est with displacements of maximum values of the order of hundred of kilometers.

Tectonic activity and seismicity are commonly attributed to the interaction of the African and European plates accompanied by a subduction process still active in the Southern part of the Peninsula. Such interpretation seems unsatisfactory since it represents only partially the dynamical processes observed. In fact, the evolution of the Apennine chain seems to be closely correlated to the opening of the Tyrrhenian Basin. Therefore only the joint analysis of the system Tyrrhenian Basin-Apennine chain enables a coherent interpretation of the spatial distribution of the regional seismicity and the expected types of mechanisms in the different seismogenetic structures.

A geodynamical model of the area that makes possibe a unitary interpretation of the opening process of the Tyrrhenian Sea, of the deformations of the Italian peninsula, of volcanism, of the seismicity of the Apennine chain and of its kinematic evolution provides for the means to define the seismotectonic model of Southern Italy.

The analysis of the tectonic evolution of the Apennine chain shows that starting from the Tortoniano the stress field acting in the area is not only caused by the convergence of the African and European plates, but also from the Tyrrhenian Sea opening. This leads to a significant movement of the Apennine system, while the actions resulted by the SE-NW subduction become less and less important. The action of the two stress fields divides the Apennine into two main arches, Northern and Southern, convex towards Foreland and separated by the line "Ortona-Roccamonfina", probably correlated to the presence of two domains, in the Tyrrhenian Basin with different expansion rate, south and north of latitude 41° respectively ((24); (46); (47); (52); (53)).

Many researchers agree in maintaining that the system Tyrrhenian Basin-Apennine chain-Foreland cannot be described in terms of simple convergence between the plates, yet it is still topic of discussion the model that can coherently interpret the coexistence of extensional processes along the inside border of the orogenic structure and compressional processes along its external border as well as the temporal migration of the entire system from West to East. In practice, we see the formation of a chain along the border not converging with the sardo-corso block and a contemporaneous opening, following behind the chain in formation, of an oceanic post collisional basin which is not easily described in terms of classic arc basin.

There are various models proposed for the opening of the Tyrrhenian Sea and for strains associated with it; therefore, it results that there are different interpretations on seismicity.

We believe that a decisive role has the uplift of the mantle in the Tyrrhenian Sea with the flux towards East. This would be endowed with active forces that involve also the surface geologic order.

The work hypothesis that we propose is that, starting from the Tortoniano, the engine of the geodynamical processes recorded in the Tyrrhenian-Apennine area is represented by the uplift of the mantle in the centre of the Tyrrhenian Sea and by its migration towards East with progressive cooling and immersion going on towards South-East, with the formation of a convective cell ((33); (34); (35); (36); (41)). Such a process leads to a significant change of the initial slab geometry in subduction from Africa to Europe which would tend at the beginning of the process to become vertical up to its dismemberment with complete inversion of the subduction process, from Europe to Africa (Fig. 13). The recent evolution of the Apennines would be linked to the opening of the Tyrrhenian Sea rather than the convergence Africa-Europa. The asthenospheric flux towards East would lead to a stress field, function of the relative velocity lythosphere-asthenosphere, able to generate crustal extension, volcanism in the Tyrrhenian Sea, migration of the Italian peninsula with tectonic thrusting towards East, extensional tectonics along the Tyrrhenian border of the chain, next to the expansion pole, and compressional towards the Foreland. This process allows us to interpret the geological structure of the chain composed of a series of detached and thrust faults towards east and northeast. The result is a very complex geometry, mainly because each tectonic phase has modified the geometrical relationships built in previous phases. Also the structure is affected by a very thick faults mesh mainly trending NW-SE and NE-SW, which makes even more complex the structural geological order.

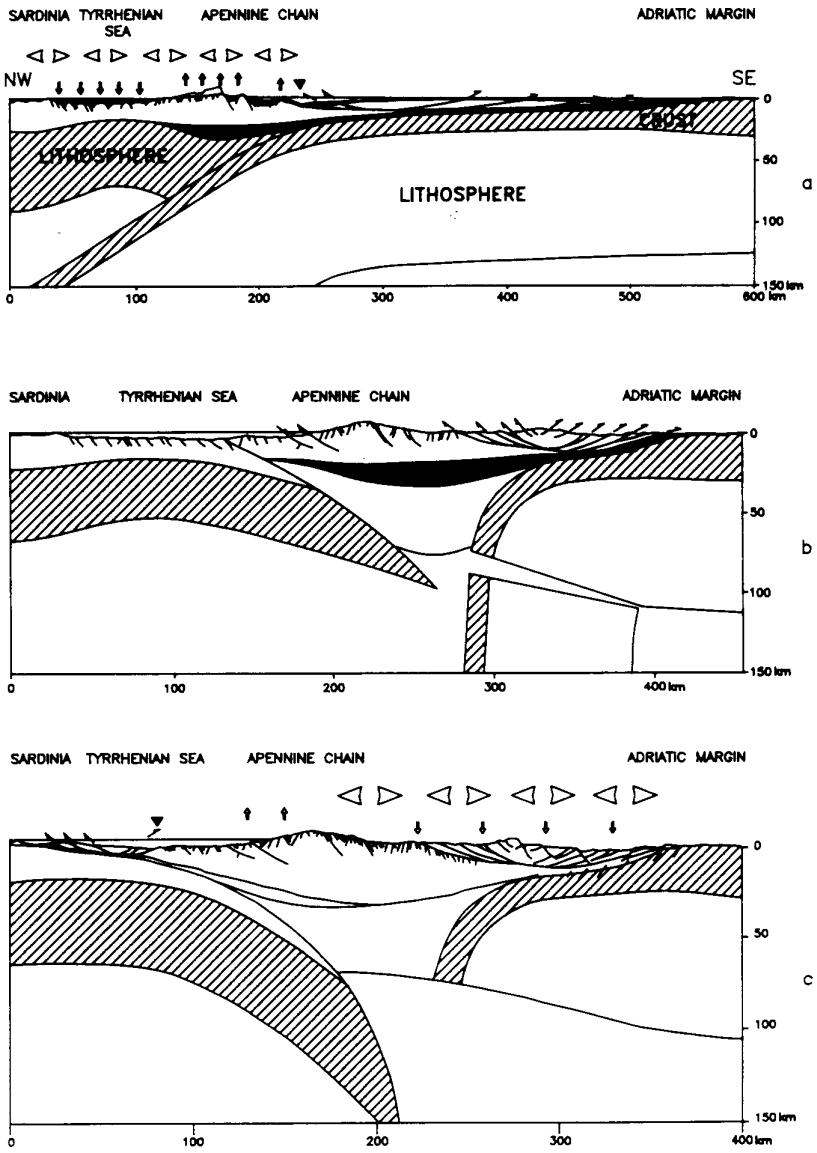

Fig. 13: A hypotetical tectonic evolution of the Southern Apennines and Tyrrhenian Basin in response tothe migration of hot masses from the asthenosphere and the continental Africa-Europe collision ((34); (35)). (a) NW-SE cross section of the Italian peninsula from the Adriatic margin to the Tyrrhenian Basin. The crust and the lithosphere boundaries are included. The Tyrrhenian basin, which is due to the spreading, and the uplift of the Apennines are shown in the upper left part of the figure. The trench is identified by a black arrow. The lower part of the sedimentary column is shown by dense lines. The continental collision produces the bending of the litosphere in the Tyrrhenian Basin. (b) Hypotetical evolution of figure a. The totality of the oceanic litosphere of the Ionian Sea has been subducted and the subduction of the thinned litosphere of the Tyrrhenian Sea begins. (c) Hypotetical evolution of figure b. Complete tectonic inversion of figure a has now occurred.

These items show the action of a stress field which produces a wide area of tension that from the Tyrrhenian Sea extends up to the first spurs of the Apennine chain, beyond Piana Campana. The main maximum strain radial with respect to Piana Abissale associated to the opening of Tyrrhenian Sea does not seem to produce at present crustal shortening and thrust faults on the front of the chain. At the most, these strains would produce strike-slip faults, trasverse to the chain. The extensional structures noticed along the axis of the chain would indicate compressional actions along the same. The latter might be associated to the onset of strains

longitudinal to the axis of the chain for the peninsula rotation (bending). Probably, it is to add to this stress field the tensile action of the residual plate in passive subduction from Ionian Sea to Tyrrhenian Sea (discoupling) that makes even more complex the field of deformations observed.

Hypothesis for a seismotectonic model

Data of historical and present seismicity show that the active structures are mainly oriented along the axis of the chain. Yet, the rupture mechanism of major magnitudo earthquakes is complex and can be interpreted by a structure longitudinal to the axis of the chain divided in segments by trasverse faults, as it has been proposed for the earthquake in Irpinia on November 23, 1980 ((9); (44); (45); (62)) and as the macroseismic field associated to the strong earthquake of Matese on December 5, 1456 would suggest.

It is commonly observed that faults of large dimensions, in case of an earthquake, do not show deformations all along their length. This result indicates that the fault would be divided in more segments that have dimensions variable from tens of kilometers up to a few hundred meters. According to seismologists the rupture propagation along the fault plane would be controlled by roughness and barriers ((1); (2)).

In the modelling of segmentation, segments persist as discrete units for long periods of time and each of them becomes deformed separately by the others. Identifying segments and their different behaviours is extremely important for long term earthquake prediction. The time elapsed between one event and the following and the return periods of earthquakes associated to each segment are parameters that can be used to assess where along the fault a great event will probably occur and to assess its probability of occurrence. This analysis provides a base to select those parts of the faulted zone where to carry out a more intensive investigation for a short term earthquake prediction.

Seismic energy release along the axis of the chain with tensile mechamisms can be associated to a compressional field with the same direction that, jointly with the expansion of Tyrrhenian Sea, contributes to the peninsula curvature.

Normal faults with Apennine direction dip both towards SW (Tyrrhenian Sea) and NE (Adriatic Sea). Faults dipping towards Tyrrhenian Sea can be associated to the residual subduction of the plate from Adriatic Sea to Tyrrhenian Sea while those dipping towards Adriatic Sea are to be associated to the migration of lithospheric masses in subduction from Tyrrhenian Sea to Adriatic ((34); (35)).

In axis of chain it cannot be excluded the action of a maximum vertical strain that could generate earthquakes with tensile mechanisms.

The deformations found in the structural analysis of the chain, show that the prevailing stress field is tensile with axis normal to the chain, and that in addition, plio-pleistocenic graben develop in connection with the chain.

Such deformations field does not seem coherent with the geodynamics of the Tyrrhenian- Apennine-Adriatic system. In fact, both the Africa-Europe relative motion and the expansion of the Tyrrhenian Sea should generate a stress field of compressional trending NE-SW. The action of this stress field might produce the tensile deformations found in axis of chain, in the hyphotesis of a bending process of the plate. In this case the upper part of the convex slab would undergo a tensile field, while in the lower part, concave, a compressional field would act; the two fields would be separated by a neutral plane (Fig. 14). In a bending process for the onset of the two stress fields, tensile and compressional, seismicity above the neutral plane should be characterized by events of a more moderate energy, compared to those localized beneath the neutral plane, but of more frequency. In this case the shallow seismicity of lower energy and more frequent, above the neutral plane, could be used as a long term precursor of the seismicity at depth localized beneath the neutral plane. The base hypothesis forsees that tensions which get gradually loaded in the slab reach the limits of rocks rupture first in the upper part and then in the lower part. A long sequence of events localized in the upper part should indicate the action of the stress field on the slab and the accumulation of tensions in depth. Major energy earthquakes will be localized at depths greater than the neutral plane and will show also longer return periods.

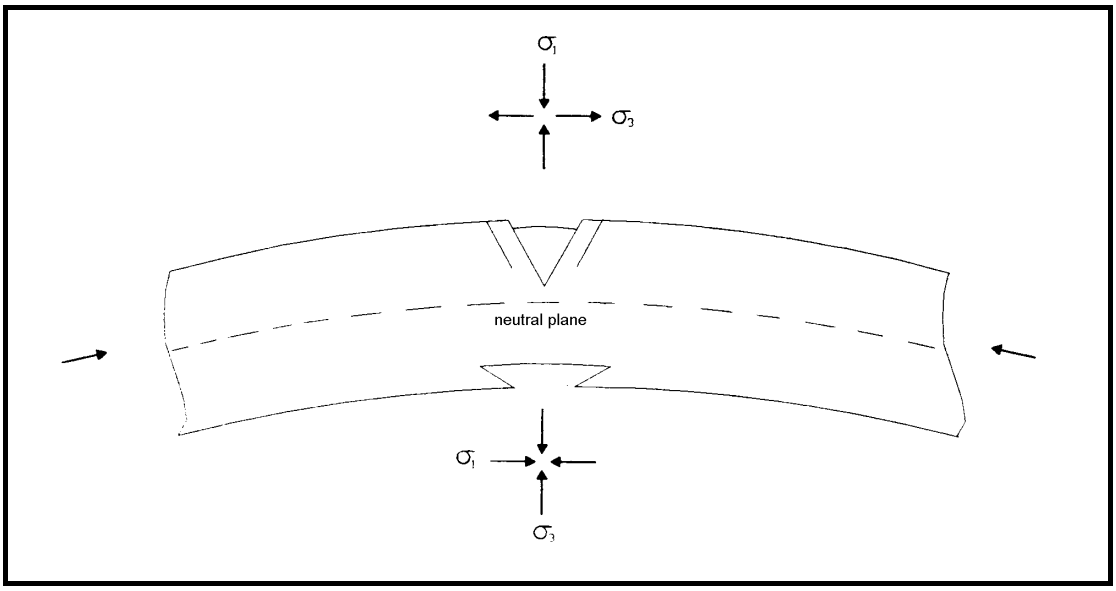

Fig. 14: Scheme of the stress field acting in a slab undergone a bending process

The tectonics of Matese shows structures longitudinal to the chain both on the Campano side and the Molisano one and transverse structures. Among these, those which delimit at NW and SE the massif along the alignments Isernia-Sesto Campano and Cerreto Sannita-Sepino are particularly important. Finally, extensional structures are responsible for the depressions of Matese Lake, Letino and Gallo. Thus it emerges a deformations field significantly complex which shows the action of a stress field as much as complex.
The historical and present seismicity shows that the active structures are mainly concentrated along the Apennine main line on Molisano side and on the Southern transverse structure, Cerreto Sannita-Sepino (Cerreto Sannita earthquake of June 5, 1688).
Also the Isernia basin is a point of tension accumulation and seismic energy release. It is not clear whether this area is to be associated only to the seismogenetic Apennine structure already mentioned, or is to be considered a nodal point between Apennine structures and anti-Apennine structures. Yet, it is to notice that the latter shows a poor present dynamics (low seismicity). Only in its expreme southern part this structure has shown recent seismicity (S. Pietro Infine-Mignano Montelungo), even if this activity could be associated with Apennine structures.
On the opposite front also Cerreto-Sannita seismicity is a kind of problem since it is not clear whether it is to be considered the boundary part of an anti-Apennine structure that delimits the Matese on the eastern side, or even enters a more external tectonic domain; in this case the Apennine structure that delimits the massif on the Campano side, would be silent from historical times.
The general cynematics of this area and the stress fields that can be outlined do not seem fully coherent with the spatial and temporal distribution of seismicity. In truth, structures that show completely similar characteristics do not release elastic energy in the same way through seismicity.
Two hypotheses can be put forward to interpret what has been observed:

- a different physical status of the medium between the Molise strip and Campania strip. According to this hypothesis the behaviour of the Molise structures would be a consequence of a rigid behaviour of the intermediate and deep crust so to allow the accumulation of elastic tensions up to the rupture with seismic energy release, while in the Campania strip it must be supposed the presence of a medium that releases tensions through a creep process;
- the accumulation of tensions in the strip currently quiet would occur with a very low increase rate such to produce seismicity with a very long return period.

The latter hypothesis was already put forward relatively to the Tyrrhenien coast strip in the realization of the preliminary seismotectonic map of the Southern Apennines (17). Such mechanism would be supported by the recent earthquake of Hanshin-Awaji (Japan) on January 17, 1995 where the earthquake would have occurred along a fault which has been silent for a thousand years. If it is possible that in the Japanese archipelago, where dynamics is very high, faults be able to reactivate themselves after a thousand years, it is to suppose that in the Italian peninsula, where dynamics is significantly lower (3-5 times), seismic silence be

able to last for a few thousands years. In such case, in the definition of a seismotectonic model, deformation processes that concern deep crust structures are to be attached a greater importance than it has been done so far.

A seismotectonic model is nothing but a tectonic model of the active structures that can generate earthquakes. Often such a model is the objective that those who work in the earthquake research field pursue and that is called " tectonic earthquake prediction". At the base of the seismotectonic model there is a cynematic model of the investigated area which must provide a reliable interpretation of the tectonic order observed as well as its temporal evolution. The joint analysis of tectonic structures and paleoseismicity, of historical and present seismicity allows to define which structures have been active in the time interval in which seismic data are available and which ones can be considered potentially active since they are structurally similar to those that the experimental datum classifies among the active ones. Once the seismotectonic model has been outlined it is possible to subdivide the investigated area in seismotectonic zones, homogenous for structural and seismicity characteristics (events energy, mechanisms, etc.). If, finally, tectonics and seismicity find also a reliable geodynamical interpretation, then one goes from seismotectonic zoning to define the seismogenetic areas.

After the earthquake occurred in Friuli in 1976, hopes for a more precise definition of seismogenetic areas were reposed in seismotectonic models. Unfortunately the results achieved so far have not met the expectations, this is likely because at the base of the research in the field there is an inadequate model of tension accumulation mechanism in the medium and of seismic energy release. In particular, the excessive simplification of the seismic source represented by a fault, could lead to wrong conclusions when one correlates seismicity with the data of tectonics. Some items provided by surface geological investigations and geophysics show structures significantly different for the parameters measured with these techniques, but which are not meaningful in relation to the processes that produce earthquakes. Basically, the experience acquired up to the present shows that the structures that produce strong earthquakes often concern areas with different tectonic structures. Therefore, as long as a more detailed model on the mechanism of earthquake will not be available, it is impossible to outline seismogenetic areas with adequate precision. A by far greater temporal problem adds to the spatial one when one wants to proceed to the reduction of seismic risk. It is evident that in order to defend ourselves from earthquakes we need to "forecast" where the future earthquake will occur and how strong it will be. A model that provides the description of what has happened is not sufficient. Instead one needs to define the stress field acting, to know geological structures, geometries of geological bodies and their mechanic characteristics.

The stress field acting at present cannot be defined only through the study of earthquakes mechanisms because the available seismic sequence does not enable to fully reconstruct the field. In fact the length of the temporal sequence of seismic events does not assure the reliability of return times of events for each seismogenetic area and does not assure that all areas able to release energies be included in seismic catalogues. Some clamorous examples support this worry. We recall the exceptional and unforecastable earthquakes of Villach in 1348, of Lisbona in 1755, of Cairo in 1992 of Kobe in 1995, only to mention a few. In such conditions adequate results for earthquakes prediction could be achieved through the following way:

- realization of the geodynamical model of the region through which it is possible to build the stress field currently acting;
- definition of a hierarchy of seismogenetic areas through the geodynamical and seismotectonic models;
- monitoring of the deformations of the suspect areas.

Since monitoring costs are high, areas at higher risk should be preferred. Therefore for monitoring, instead of more active areas, one should give preference to those areas that can produce more damages.

References

(1) AKI K. (1979) - Characterization of barriers on an earthquake fault. J.Geophys.Res., 84, 6140-6148.

(2) AKI K. (1984) - Asperities, barriers, and characteristic earthquakes. J. Geophys. Res., 89, 5867-5872.

(3) ALBERTI G., ESPOSITO S. and VETRELLA S., 1994: The Vesuvius DEM: a test case for the TOPSAR system. Proc. of the Final Results Workshop "MAC-Europe 91",Lenggries, Germany, pp. 49-55.

(4) ALESSIO G., GODANO C., GORINI A., RICCIARDI G.P. (1987) - Studio della sequenza sismica del gennaio 1986 presso Isernia. Mem. Soc.Geol. Ital., 37, 253-266.

(5) ALESSIO G., FERRI M., GORINI A., LUONGO G. (1988) - Sismicità dell'Appennino Meridionale nel periodo 1982-87. Memorie Soc.Geol.It., XLI, 1129-1137.

(6) ALESSIO G., ESPOSITO E., GORINI A., LUONGO G., PORFIDO S. (1993) - Identification of seismogenic areas in the Southern Apennines, Italy. Annali di Geofisia, Vol. XXXVI, n.1, 227-235.

(7) ALESSIO G., GORINI A., VILARDO G., IANNACCONE G. (1995) - Low energy sequences in areas with high seismic potential: Benevento (Southern Apennines), April 1990. Natural Hazard (In press).

(8) BARBANO M.S., EGOZCUE J.J., GARCIA FERNANDEZ, KIJKO A., LAPAJNE J., MAYER-ROSA D., SCHENK V., SCHENKOVA Z., SLEJKO D., ZONNO G. (1989) - Assessment of seismic hazard for the Sannio Matese area of Southern Italy - A summary. Natural Hazard,2, 217-228.

(9) BERNARD P., ZOLLO A., TRIFU CEZAR-IOAN, HERRERO A. (1993) - Details of the rupture kinematics and mechanism of the 1980 Irpinia earthquake: new results and remaining questions. Annali di Geofisica, Vol. XXXVI, n.1, 71-80

(10) BOUSQUET J.C., GRELLET B., SAURET B. (1993) - Neotectonic setting of the Benevento area: comparison with the epicentral zone of the Irpinia earthquake. Annali di Geofisica, Vol. XXXVI, n.1, 245-251.

(11) BRANNO A, ESPOSITO E., LUONGO G., MARTURANO A., PORFIDO S., RINALDIS V. (1986) - The largest earthquakes of the Apennines, Southern Italy, IAEG, AIG Proc of the Intern. Symp. on Engineering Geology Problems in Seismic Areas - Bari, Italy, IV, 3-14.

(12) BRUZZI S., GUIGNARD J.-P., PIKE T., 1982, "Quality assessmant of remote-sensing data: the SAR case", ESA Journal, 1982, vol.6, pp. 271-281.

(13) CELLO G., GUERRA I., TORTORICI L., TURCO E. & SCARPA R. (1982) - Geometry of the neotectonic stress field in southern Italy: geological and seismological evidence. Journal of Structural Geology, 4, n.4, 385-393.

(14) CHIARUTTINI C.& SIRO L. (1991). Focal mechanism of an earthquake of Baroque age in the 'Regno delle due Sicile' (Southern Italy). Tectonophysics, 193: 195-203.

(15) CUBELLIS E., DEL GAUDIO C., GRIMALDI M., RICCO C., LUONGO G. (1989) - La rete gravimetrica per il controllo della dinamica della Piana Campana. Pubbl.n.1/89, Osservatorio Vesuviano, Napoli.

(16) CUBELLIS E., DEL GAUDIO C., FERRI M., GRIMALDI M., OBRIZZO F., RICCO C., LUONGO G. (1991) - Gravity anomalies in the Campanian Plain (Southern Italy) and their volcano-tectonic implications. Acta Vulcanologica, Vol.1, 57-62.

(17) DE VIVO B., DIETRICH D., GUERRA I., IANNACCONE G., LUONGO G., SCANDONE P., SCARPA R., TURCO E. (1979) - Carta sismotettonica preliminare dell'Appennino Meridionale. Pubblicazione n.166 del Consiglio Naz.Ricerche - Progetto Finaliz. Geodinamica.

(18) DEWEY J.F., HELMAN M.L., TURCO E., HUTTON D.H. W. & KNOTT S.D. (1989) - Kinematics of the western Mediterranean. In : "Alpine Tectonics" Coward M.P., Dietrich D. & Park R.G. (Eds). Geological Society Special Pubblication n.45, 265-283.

(19) DOWMAN I., 1992:The geometry of SAR images for geocoding and stereo applications. Int. J. Remote Sensing, vol. 13, no. 9, pp. 1609-1617.

(20) ESPOSITO E., LUONGO G., MARTURANO A. & PORFIDO S. (1987) - Il terremoto di S.Anna del 26 luglio 1805. Mem.Soc.Geol.It., 37, 171-191

(21) FEDERICI P., DI MARO R., MARCHETTI A., COCCO M. (1992). Analisi della sismicità dell'area del Sannio-Matese negli anni 1991-1992.Atti 11° Convegno Ann. GNGTS, CNR,, I:389-404.

(22) FERRI M., LUONGO G., OBRIZZO F., SANTAMARIA R., TROISI S. (1994) - Monitoraggio dei movimenti del suolo nella Piana Campana con tecnica GPS" Boll. Soc. It., Topografia e Fotogrammetria, Vol. 1, pp.123-136.

(23) FIGLIUOLO B. (1988) - Il terremoto del 1456. Ed.Studi Storici Meridionali. Salerno.

(24) FINETTI I. & DEL BEN A. (1986) - Geophysical study of the Tyrrhenian opening. Boll. Geofis.Teor.Appl., 28, 75-155.

(25) GABRIEL A. K., GOLDSTEIN R. M., ZEBKER H. A., "Mapping small elevation changes over large areas: differential radar interferometry", J. Geophys. Res., vol. 94, no. B7, pp. 9183-9191, 1989.

(26) GASPARINI C., IANNACCONE G., SCARPA R. (1985). Fault-plane solutions and seismicity of the italian peninsula. Tectonophysics, 117, 59-78.

(27) GOLDSTEIN R.M., ZEBKER H.A. and WERNER C.L., 1988: Satellite radar interferometry: Two-dimensional phase unwrapping. Radio Science, vol. 23, no. 4, pp. 713-720.

(28) HIPPOLYTE J.C., ANGELIER J., ROURE F. (1994) - A major geodynamic change revealed by Quaternary stress patterns in the Southern Apennines (Italy). Tectonophysics, 230, 199-210.

(29) LAPAJNE J., BRESKA Z., GODEC M. & ZIVICIC M. (1989) - Seismic hazard in the Sannio-Matese Area of Italy. Natural Hazard, 2, 363-385.

(30) LAVECCHIA G. (1988) - The Tyrrhenian-Apennines system: structural setting and seismotectogenesis. Tectonophysics, 147, 263-296.

(31) LI F.K., GOLDSTEIN R. M., "Studies of multibaseline spaceborn interferometric synthetic aperture radars", IEEE Trans. on Geoscience and Remote Sensing, vol. 28, no.1, Jan. 1990, pp.88-97.

(32) LOCARDI E. (1988) - Geodinamica attuale dell'Appennino. In : L'Appennino campano lucano nel quadro geologico dell'Italia meridionale. Atti 74° Congresso Nazionale della Soc.Geol.Ital., 88-92.

(33) LUONGO G. (1988) - Tettonica Globale dell'Italia Meridionale: Subduzione o Bending? Mem.Soc.Geol.It., 41, 159-163.

(34) LUONGO G., CUBELLIS E., OBRIZZO F. & PETRAZZUOLI S.M. (1991 a) - A physical model for the origin of volcanism of the Tyrrhenian margin: the case of Neapolitan area. Journal of Volcanology and Geoth.Res., 48, 173-185.

(35) LUONGO G., CUBELLIS E., FERRI M., OBRIZZO F. & TORTORA A. (1991 b) - E' falsificabile il modello della Tettonica Globale? Il caso dell'Italia Meridionale. Mem.Soc.Geol. It., 47, 333-340.

(36) LUONGO G., CUBELLIS E., OBRIZZO F., PETRAZZUOLI S.M. (1991 c) - Modello fisico per l'origine del vulcanismo del margine tirrenico. Extended Abstract, Atti X Convegno GNGTS, Vol.II, 885-888.

(37) LUONGO G., CUBELLIS E., FERRI M., MARTURANO A., MILANO G., OBRIZZO F.(1992) - A seismotectonic model of Southern Apennines and Tyrrhenian Basin. Poster Session 29th International Geological Congress, Kyoto, Japan, 24 Aug.-3 Sept. 1992.

(38) LUONGO G., MARTURANO A., RINALDI V. (1993) - Macroseismic data: present limits and future possibilities. Annali di Geofisica, Vol.XXXVI, n.1, 293-299.

(39) MAYER-ROSA D. (1989) - Critical parameter investigation for earthquake hazard assessment in the Sannio-Matese Area of Southern Italy. Natural Hazard, 2, 237-247.

(40) MAYER -ROSA D., SLEJKO D., ZONNO G. (1993) - Assessment of seismic hazard for the Sannio-Matese area, Southern Italy (Project "TERESA"). Annali di Geofisica, Vol. XXXVI, n.1, 199-209.

(41) MILANO G., VILARDO G. & LUONGO G. (1994) - Continental collision and basin opening in Southern Italy: a new plate subduction in the Tyrrhenian Sea? Tectonophysics, 230, 249-264.

(42) MOCCIA A., ESPOSITO S., D'ERRICO M.: "Height Measurement Accuracy by ERS-1 SAR Interferometry",International Workshop on SAR Interferometry, Napoli, 1993, EARSeL Advances in Remote Sensing, vol 3, no.1, September 1994.

(43) NERI G. & WYSS M. (1993). Preliminary results fron stress tensor inversion of earthquake fault-plane solutions in the Southern Tyrrhenian Region. Boll.Geof.Teor.Appl., XXXV, n.139: 349-362.

(44) PANTOSTI D. & VALENSISE G. (1993) - Source geometry and long-term behavior of the 1980, Irpinia earthquake fault based on field geologic observations. Annali di Geofisica, Vol.XXXVI, n.1, 41-50.

(45) PANTOSTI D., D'ADDEZIO G., CINTI F.R. (1993) - Paleosismological evidence of repeated large earthquakes along the 1980 Irpinia earthquake fault. Annali di Geofisica, Vol.XXXVI, n.1, 321-330.

(46) PATACCA E. & SCANDONE P. (1987) - Tectonic Evolution of the outer margin of the Apennines and related foredeep system. Boriani A. et al., Editors, "The litosphere in Italy Advances in earth science research. Accademia Nazionale dei Lincei.

(47) PATACCA E., SARTORI R., SCANDONE P. (1990) - Tyrrhenian Basin and Apenninic Arcs: Kinematic Relations Since Late Tortonian Times. Mem.Soc.Geolo.It., 45, 425-451.

(48) POSTPISCHL D. (Editor) - (1985 a) - Atlas of isoseismal maps of italian earthquakes. Quaderni de "La Ricerca Scientifica" del CNR, n.114, Vol 2A.

(49) POSTPISCHL D. (Editor) (1985 b) - Catalogo dei terremoti italiani dall'anno 1000 al 1980. Quaderni de "La Ricerca Scientifica" del CNR, n.114, Vol.2B.

(50) PRATI C., ROCCA F., 1990, "Limits to the resolution of elevation maps from stereo SAR images", Int. J. of Remote Sensing, vol. 11, no. 12.

(51) PRATI C., ROCCA F., AND MONTI GUARNIERI (1993), "SAR Interferometry Experiments with ERS-1", Proceeding First ERS-1 Symposium, pp. 211-218.

(52) ROYDEN L., PATACCA E., SCANDONE P. (1987) - Segmentation and configuratio of subducted lithosphere in Italy: An important control on trust-belt and foredeep-basin evolution. Geology, 15, 714-717.

(53) SCANDONE P., PATACCA E., MELETTI C., BELLATALLA M., PERILLI N., SANTINI U. (1990) - Struttura geologica, evoluzione cinematica e schema sismotettonico della penisola italiana. Atti del Convegno GNDT vol.1, 119-135.

(54) SCARPA R. (1990) - Analisi dei meccanismi focali: problematiche ed applicazioni ai terremoti italiani. Att. convegno GNDT-CNR, Vol.1, 137-156.

(55) SIRO L. & SLEJKO D. (1989) - Different Approaches to the Seismic hazard of Sannio-Matese (Southern Italy). Natural Azard, 2, 329-348.

(56) SMALL D., WERNER C.L. AND NÜESCH D., 1993: Baseline Modeling for ERS-1 SAR Interferometry. Proc. of Int. Geoscience and Rem. Sens. Symp., Tokyo, Japan, pp. 1204-1206.

(57) SMALL D., WERNER C.L. AND NÜESCH D., 1995:Geocoding and validation of ERS-1 InSAR-derived digital elevation models. EARSeL Advances in Remote Sensing, vol.4, no. 2, pp. 26-39.

(58) SUHADOLC P., PANZA G.F., MARSON I., COSTA G., VACCARI F. (1990) - Analisi della sismicità e meccanismi focali nell'area italiana. Atti del Convegno GNDT "Zonazione e riclassificazione sismica", vol.I, 157-168.

(59) UNGUENDOLI M. (1992) - La tecnica GPS in Italia: stato dell'arte e prospettive future. Bollettino SIFET, n.1.

(60) WERNER C.L., GOLDSTEIN R.M., ROSEN P. AND ZEBKER H.A., 1992. "Techniques and Applications of SAR Interferometry for ERS-1: Topographic Mapping, Slope Measurement and Change Detection", Proc. of 1st Workshop ERS-1 Fringe Working Group, ESA ESRIN, Frascati, pp. 11.

(61) WESTAWAY ROB (1987) - The Campania, southern Italy, earthquakes of 1962 August 21. Geophys. J. R. Astr. Soc., 88, 1-24.

(62) WESTAWAY ROB (1993) - Fault rupture geometry for the 1980 Irpinia earthquake: a working hypothesis. Annali di Geofisica, Vol.XXXVI, n.1, 51-69.

(63) ZEBKER H. A., WERNER C. L., ROSEN P. A., AND HENSLEY S. (1994). "Accuracy of Topographic Maps Derived from ERS-1 Interferometric Radar", IEEE Transactions on Geoscience and Remote Sensing, Vol. 32, NO. 4, 823-836.